Development/Plasticity/Repair

EBF1 Limits the Numbers of Cochlear Hair and Supporting Cells and Forms the Scala Tympani and Spiral Limbus during Inner Ear Development

Hiroki Kagoshima,[1] Hiroe Ohnishi,[1] Ryosuke Yamamoto,[2] Akiyoshi Yasumoto,[1] Yosuke Tona,[1] Takayuki Nakagawa,[1] Koichi Omori,[1] and Norio Yamamoto[1,3]

[1]Department of Otolaryngology, Head and Neck Surgery, Graduate School of Medicine, Kyoto University, Kyoto 606-8507, Japan, [2]Biological Sciences, Sunnybrook Research Institute, Sunnybrook Health Sciences Centre, Toronto, Ontario M4N 3M5, Canada, and [3]Department of Otolaryngology, Kobe City Medical Center General Hospital, Hyogo 650-0047, Japan

Early B-cell factor 1 (EBF1) is a basic helix–loop–helix transcription factor essential for the differentiation of various tissues. Our single-cell RNA sequencing data suggest that *Ebf1* is expressed in the sensory epithelium of the mouse inner ear. Here, we found that the murine *Ebf1* gene and its protein are expressed in the prosensory domain of the inner ear, medial region of the cochlear duct floor, otic mesenchyme, and cochleovestibular ganglion. *Ebf1* deletion in mice results in incomplete formation of the spiral limbus and scala tympani, increased number of cells in the organ of Corti and Kölliker's organ, and aberrant course of the spiral ganglion axons. *Ebf1* deletion in the mouse cochlear epithelia caused the proliferation of SOX2-positive cochlear cells at E13.5, indicating that EBF1 suppresses the proliferation of the prosensory domain and cells of Kölliker's organ to facilitate the development of appropriate numbers of hair and supporting cells. Furthermore, mice with deletion of cochlear epithelium-specific *Ebf1* showed poor postnatal hearing function. Our results suggest that *Ebf1* is essential for normal auditory function in mammals.

Key words: **early B-cell factor 1; hearing; inner ear prosensory domain; Kölliker's organ; scala tympani; spiral limbus**

Significance Statement

The elaborate cellular organization and three-layered luminal structure of the mammalian cochlea are essential for normal sound perception, but the developmental process of these structures is not fully understood. The present study revealed the roles of the basic helix–loop–helix type transcription factor *Ebf1* in the development of the cochlea. *Ebf1* was widely expressed in the inner ear, regulated the proper number of cochlear hair and supporting cells, and was involved in developing scala tympani and spiral limbus. As a result, *Ebf1* was necessary for the development of normal hearing. These results suggest the essential roles of *Ebf1* in the whole cochlear development and contribute to understanding a part of the complex cochlear development process.

Introduction

The inner ear is a unique and complex organ that consists of bony and membranous labyrinths. The membranous labyrinth contains multiple sensory organs, including the cochlea and several vestibular organs. The cochlea is responsible for hearing and comprises three compartments (scalae): the scala vestibuli, scala tympani, and scala media. The scala vestibuli and scala tympani develop from the mesenchyme surrounding the inner ear (Sher, 1971). The scala media is situated between the scala vestibuli and scala tympani and contains sensory epithelia that transduce sound into electrical signals via specialized sensory cells known as hair cells. Cochlear hair cells are located within the organ of Corti in the middle part of the scala media epithelium and consist of one row of inner hair cells and three rows of outer hair cells. These hair cells are surrounded by several types of nonsensory supporting cells, including pillar and Deiters' cells. The precise number and placement of mechanosensory hair cells and nonsensory supporting cells enable the accurate reception of mechanical stimulation of sound and its conversion into neural signals.

Received June 7, 2023; revised Nov. 12, 2023; accepted Dec. 13, 2023.

Author contributions: H.O. and N.Y. designed research; H.K., H.O., R.Y., A.Y., Y.T., T.N., and K.O. performed research; H.K., A.Y., and N.Y. analyzed data; H.K. and N.Y. wrote the paper; H.K. and N.Y. wrote the first draft of the paper; N.Y. edited the paper.

We thank Dr. Rudolf Grosschedl for providing *Ebf1*$^{-/-}$ and *Ebf1*$^{fl/fl}$ mice, Dr. Ryoichiro Kageyama for providing the *Atoh1* ISH probe, and Center for Anatomical, Pathological and Forensic Medical Research, Graduate School of Medicine, Kyoto University for preparing hematoxylin–eosin staining slides. This study was supported by Japan Society for the Promotion of Science KAKENHI (grant number: JP22H03234) awarded to N.Y.

The authors declare no competing financial interests.

Correspondence should be addressed to Norio Yamamoto at yamamoto@ent.kuhp.kyoto-u.ac.jp.

https://doi.org/10.1523/JNEUROSCI.1060-23.2023

Inner ear development in mice begins with the formation of an ectodermal thickening called the otic placode, which is located adjacent to the hindbrain (Wu and Kelley, 2012). The otic placode invaginates to form a spherical structure called an otocyst at approximately embryonic day (E) 9.5. The ventral side of the otocyst forms the future sensory epithelium, where the sex-determining region Y-box transcription factor 2 (*Sox2*) is expressed (Kiernan et al., 2005). At E10.5, the cochlear and endolymphatic ducts and semicircular canals begin to form on the ventral and dorsal sides of the otocyst, respectively. The ventral side of the cochlear duct (cochlear duct floor) begins to develop into a future sensory domain by expressing *Sox2* and *Jagged1* at E11.5 (Wu and Kelley, 2012). The *Sox2*-positive region becomes limited to the middle part of the ventral cochlear duct and is recognized as a prosensory domain at E13.5 and E14.5 (Kiernan et al., 2005; Ohyama et al., 2010). The region medial to the prosensory domain toward the axis of the cochlea (modiolus) is called the greater epithelial ridge (GER) and transiently contains Kölliker's organ, which is composed of columnar supporting cells during the developmental stage and becomes the inner sulcus with cuboidal cells and the spiral limbus with interdental cells in the mature cochlea (Dayaratne et al., 2014). Additionally, the GER is a source of sensory epithelia and has the potential to produce sensory cells after the establishment of hair cells (Kubota et al., 2021).

The complex cellular structure and developmental processes of the inner ear depend on the highly regulated expression patterns of signaling molecules and transcription factors. However, the mechanisms underlying inner ear development are not fully understood. To comprehensively elucidate these mechanisms, we analyzed the single-cell RNA-seq data of the inner ear epithelial cells. In this study, we found that the early B-cell factor 1 gene (*Ebf1*) was upregulated in clusters of sensory epithelial progenitors and confirmed that it was expressed on the medial side of the cochlear duct floor, the prosensory area of the vestibular macula and crista, and the spiral ganglion (Yamamoto et al., 2021).

EBF1 belongs to the EBF family of transcription factors, which are basic helix–loop–helix (bHLH) transcription factors (Hagman et al., 1995), and encodes four paralogous genes in mammals (Liberg et al., 2002). Similar to other bHLH transcription factors, EBF1 is involved in various developmental processes, including the determination of cell fate and differentiation of B-lymphocytes and olfactory epithelia (Liberg et al., 2002).

Considering the various roles of EBF1 as a bHLH transcription factor and the importance of bHLH transcription factors—such as ATOH1—in inner ear development, we analyzed the function of EBF1 in inner ear development. In the present study, we confirmed the spatiotemporal expression of *Ebf1* during inner ear development and examined the effects of *Ebf1* deletion on inner ear development and hearing.

Material and Methods

Animals. Slc: ICR mice were purchased from Japan SLC. $Ebf1^{-/-}$ mice (Lin and Grosschedl, 1995) and $Ebf1^{fl/fl}$ (Gyory et al., 2012) were used in this study. $Ebf1^{fl/+}$ mice were crossed with $Foxg1^{Cre/+}$ *mice* (*Foxg1Cre*; Hébert and McConnell, 2000), and $Ebf1^{-/-}$ or *Foxg1Cre;*$Ebf1^{fl/fl}$ mice were used as experimental animals. Additionally, we used $Ebf1^{+/+}$ and $Ebf1^{+/-}$ mice as controls of $Ebf1^{-/-}$ mice and *Foxg1Cre;*$Ebf1^{fl/+}$ mice as controls of *Foxg1Cre;*$Ebf1^{fl/fl}$ mice.

$Ebf1^{+/-}$, *Foxg1Cre*, and $Ebf1^{fl/fl}$ mice were maintained on a C57BL/6 background. All experimental protocols were approved by the Animal Research Committee of Kyoto University (Med Kyo 20132, Kyoto, Japan). All animal experiments were performed according to the National Institutes of Health Guidelines for the Care and Use of Laboratory Animals. All the animals used in this study were maintained at the Institute of Laboratory Animals, Graduate School of Medicine, Kyoto University. The mice were mated in the evening, and vaginal plugs were checked early in the morning. The day a vaginal plug was detected was defined as E0.5.

Quantitative reverse transcription polymerase chain reaction. Inner ears were dissected from E9.5, E10.5, E11.5, E12.5, E13.5, E14.5, E16.5, E18.5, and postnatal day (P) 0 ICR mice. After the surrounding tissue was removed from the inner ears, at least four samples were immersed in TRIzol Reagent (15596018, Thermo Fisher Scientific) and preserved at −80°C until RNA extraction. Total RNA was extracted using the RNeasy Mini Kit (74104, QIAGEN) and reverse transcribed using the ReverTra Ace qPCR RT Master Mix with gDNA Remover (FSQ-301, TOYOBO). The cDNA was mixed with PowerUp SYBR Green Master Mix (A25742, Applied Biosystems) and various sets of gene-specific forward and reverse primers and subsequently subjected to real-time PCR quantification using a StepOnePlus Real-Time PCR System (4376373, Applied Biosystems). The following primer sequences were used: *Ebf1* forward, AACTCCAAGCACGGGCGGAG; *Ebf1* reverse, CGGGCT GATGGCTTTGATACAGG; *Rplp0* forward, CACTGGTCTAGG ACCCGAGAAG; *Rplp0* reverse, GGTGCCTCTGGAGATTTT CG. Relative mRNA expression levels were calculated using the standard curve method, and the mouse housekeeping gene *Rplp0* was used as an invariant control.

In situ hybridization. Whole embryos (E9.5–E11.5) and whole heads (E12.5–P0) were fixed in 4% paraformaldehyde (PFA; 02890-45, Nacalai Tesque) in 0.1 M phosphate-buffered saline (PBS; 162-19321, FUJIFILM Wako Pure Chemical Corporation) at 4°C overnight. Samples were cryoprotected in 30% sucrose (30403-55, Nacalai Tesque)/PBS, embedded in Tissue-Tek O.C.T. compound (4583, Sakura Finetek Japan), and sectioned at 10 µm thickness using a cryostat (CryoStar NX70; MIC956960, Thermo Fisher Scientific). The sections were subsequently mounted on silane-coated glass slides (SMAS-01, Matsunami Glass).

cDNA fragments were generated by PCR using E13.5 inner ear cDNA of Slc:ICR mice and subsequently cloned into the pCR-Blunt II-TOPO vector (451245, Invitrogen) to prepare RNA probe templates. We synthesized digoxigenin (DIG)-labeled sense and antisense RNA probes using a DIG RNA Labeling Kit (11175033910, Roche) after digestion with the appropriate restriction enzymes *Bam*HI-HF, *Hind*III, *Not*I-HF, *Sac*I, or *Xho*I (R3136S, R0104S, R3189S, R0156S, R0146S, New England Biolabs). The following probes were used for in situ hybridization (ISH): *Ebf1* (NM_001,290,709, nucleotides 1436–2269), *Sox2* (IMAGE clone: 6413283), *Bmp4* (NM_007554.3, nucleotides 1013–1876), *Atoh1* (NM_007500.5, nucleotides 13–2111), and *Fgf10* (NM_008002.5, nucleotides 571–1027). Each corresponding sense probe was used as a negative control.

Sections were fixed with 4% PFA and 0.2% glutaraldehyde (17025-25, Nacalai Tesque) in PBS at room temperature (RT) for 10 min, bleached with 6% hydrogen peroxidase (081-04215, FUJIFILM Wako Pure Chemical Corporation) in 0.1% Tween 20 (sc-29113, Santa Cruz Biotechnology) in PBS (PBST) at RT for 10 min, treated with 20 µg/µl proteinase K (3115879001, Roche) for 5 min, and refixed with 4% PFA and 0.2% glutaraldehyde in PBS at RT for 10 min.

The prehybridization was performed in hybridization solution containing 50% formamide (13015-75, Nacalai Tesque); 5× saline sodium citrate buffer, adjusted to pH 4.5 with citrate (SSC, 32146-91, Nacalai Tesque); 1% sodium dodecyl sulfate (71736-500ML, Sigma-Aldrich); 50 µg/ml yeast RNA (AM7118, Invitrogen); and 50 µg/ml heparin (H9399-100KU, Sigma-Aldrich) at 70°C for 1 h. For hybridization, we incubated the sections in a hybridization solution with a 0.2 µg/ml DIG-labeled RNA probe at 70°C for 16 h in sealed plastic bags.

Sections were rinsed first in 50% formamide with 6× SSC and 1% sodium dodecyl sulfate at 70°C, then in 50% formamide with 2.4× SSC at 65°C, and finally in 1× Tris-buffered saline (35438-81, Nacalai Tesque) with 0.1% Tween 20 (TBST) at RT. Sections were blocked with 5% sheep serum (S2263-500ML, Sigma-Aldrich) and incubated with a 1:4,000 dilution of anti-digoxigenin-AP Fab fragments (11093274910, Roche) at 4°C overnight.

After rinsing with TBST and NTMT containing 100 mM NaCl (31334-51, Nacalai Tesque), 100 mM Tris-HCl, pH 9.5, 10 mM $MgCl_2$ (133-00161, FUJIFILM Wako Pure Chemical Corporation), 0.1% Tween 20, and 480 µg/ml levamisole (16595-80-5, Sigma-Aldrich), the sections were incubated with nitro-blue tetrazolium chloride (11383213001, Roche) and 5-bromo-4-chloro-3-indolyl phosphate solution (B6777-100MG, Roche). Images were captured using a BX50 microscope (Olympus).

Immunohistochemistry analysis. Immunohistochemistry (IHC) sections were prepared in a manner similar to that used for ISH. After washing with PBS, all samples were incubated with Blocking One Histo (06349-64, Nacalai Tesque) for 10 min at RT and 10% normal donkey serum (D9663-10ML, Sigma-Aldrich) in PBS/0.5% Triton X-100 with 5% Blocking One Histo for 30 min at RT. The samples were stained with primary antibodies at 4°C overnight or RT for 1 h. After washing with PBST, the samples were incubated with Alexa Fluor secondary antibodies. F-actin (actin filaments) was stained with phalloidin 647 (1:500; A22287, Thermo Fisher Scientific) at RT for 1 h. Nuclei were stained with 4′,6-diamidino-2-phenylindole (DAPI; D1306, Thermo Fisher Scientific).

The following primary antibodies were used in this study: rabbit anti-EBF1 antibody (1:1,000, AB10523, RRID: AB_2636856; Millipore), mouse anti-MYO7A antibody (1:1,000, 138-1; Developmental Studies Hybridoma Bank), rabbit anti-MYO7A antibody (1:1,000, 25-6790, RRID: AB_10015251; Proteus BioSciences), goat anti-SOX2 antibody (1:250, AF201, RRID: AB_355110; R&D Systems), rabbit anti-SOX2 antibody (1:100, 11064-1-AP, RRID: AB_2195801; Proteintech), rabbit anti-VGLUT3 antibody (1:500, 135 203, RRID:AB_887886; Synaptic Systems), goat anti-JAG1 antibody (1:500, sc-6011, RRID: AB_649689; Santa Cruz Biotechnology), mouse anti-p27Kip1 antibody (1:200, 610242, RRID: AB_397637; BD Biosciences), rabbit anti-Tubulin β 3 (TUJ1) antibody (1:1000, PRB-435P, RRID: AB_291637; BioLegend), rabbit anti-PROX1 antibody (1:500, AB5475, RRID: AB_177485; Millipore), rabbit Anti-Nerve Growth Factor Receptor Antibody, p75 antibody (1:500, AB1554, RRID: AB_11211656; Millipore), rabbit anti-BLBP (FABP7) antibody (1:200, ab32423, RRID: AB_880078; Abcam), and rabbit anti-cleaved caspase 3 (Asp175) antibody (1:400, 9661, RRID: AB_2341188; Cell Signaling Technology).

Antigen retrieval was performed for CDKN1B (mouse anti-p27Kip1 antibody) staining by heating sections in HistoVT One (06380-76, Nacalai Tesque) at 90°C for 10 min prior to the addition of the primary antibodies.

The secondary antibodies used were Alexa Flour 488 donkey anti-rabbit IgG, Alexa Flour 488 donkey anti-goat IgG, Alexa Flour 488 donkey anti-mouse IgG, Alexa Flour 568 donkey anti-rabbit IgG, Alexa Flour 568 donkey anti-goat IgG, Alexa Flour 647 donkey anti-rabbit IgG, Alexa Flour 647 donkey anti-goat IgG, and Alexa Flour 647 donkey anti-mouse IgG (1:500; A21206, A11055, A21202, A10042, A11057, A31573, A21447, A31571, Thermo Fisher Scientific).

The sections were mounted using Fluoromount-G Anti-Fade (0100-35, Southern Biotechnology Associates). Images of the specimens were captured using an Olympus BX50 microscope (Olympus), an Olympus DP70 digital camera (Olympus), and a Zeiss LSM900 with Airyscan2 (Carl Zeiss).

Hematoxylin–eosin staining. Freshly isolated E18.5 mouse heads were immediately fixed by 10% formaldehyde and embedded in paraffin. Paraffin sections (3 µm thick) were immersed in hematoxylin monohydrate (1.15938, Sigma-Aldrich) at RT for 7.5 min and in eosin Y (115935, Sigma-Aldrich) at RT for 2 min. Dehydration was performed using graded ethanol solutions (70%, 90%, and three times 100%), and clearing was performed three times using xylene.

Cochlea whole-mount preparation. The inner ears were dissected from mice heads at E18.5 and fixed in 4% PFA in PBS at RT for 1 h. After fixation and before primary antibody staining, the outer membrane, including Reissner's membrane, was removed to expose the organs of Corti. After staining with a secondary antibody, the organ of Corti was dissected and mounted on a glass slide for imaging.

Proliferation and apoptosis assays. Cell proliferation in the cochlea was assessed by detecting the incorporated 5-ethynyl-2′-deoxyuridine (EdU; A10044, Thermo Fisher Scientific) on frozen sections. EdU was detected using the Click-iT Plus EdU Cell Proliferation Kit for Imaging Alexa 555 Dye (C10638, Thermo Fisher Scientific), according to the manufacturer's instructions. Pregnant mice were injected with EdU at E12.5, E13.5, and E14.5 (three injections at 50 µg/g at 2 h intervals) and at E16.5 (a single injection at 100 µg/g). E12.5, E13.5, and E14.5 embryos were collected 8 h after the first injection. E16.5 embryos were collected 4 h after the injection. The basal or basal-to-middle regions of the cochlear duct were observed at E12.5 or at E13.5, E14.5, and E16.5, respectively.

Apoptotic cells were detected by identifying the expression of cleaved caspase 3 (CC3) in frozen sections via IHC staining.

Auditory brainstem response and distortion product of otoacoustic emissions. Auditory brainstem response (ABR) measurements were performed under general anesthesia as described previously (Kada et al., 2009) at P21 ($n = 3$ for each genotype). The thresholds for 10, 20, and 40 kHz were determined based on the responses at different intensities with 5 dB sound pressure level intervals. Distortion product of otoacoustic emission (DPOAE) recordings were performed as described previously (Hamaguchi et al., 2012) at P21 ($n = 4$ for each genotype). Two primary tones (f1, f2, f1 < f2) were used as input signals, with f2 set at eight frequency points (4, 6, 8, 12, 16, 24, 32, and 40 kHz), maintaining a frequency ratio of f2/f1 = 1.2. The intensity levels of the stimulatory sounds were 65 and 55 dB sound pressure levels for f1 and f2, respectively. DPOAE was detected as a peak at 2f1–f2 in the spectrum.

Quantification. Cell quantification and measurements were performed at E18.5 using the Cell Counter plugin of ImageJ

(Schneider et al., 2012). The total length of the cochlea was measured based on the region with MYO7A-positive hair cells from the basal to apical turns. Cochlear hair cells were identified by phalloidin and MYO7A labeling. Two types of cells, PROX1- and SOX2-positive cells, were counted to quantify the supporting cells of the cochlea. The cochlear duct was divided into three regions, basal, middle, and apical, and we selected the 200 μm length in each region for MYO7A- and PROX1-positive cells and 100 μm in the basal region for SOX2-positive cells from the center part of each region and counted the number of cells within the selected part. To determine the number of cochlear hair cells and supporting cells in the entire length of the cochlea, we counted the number of MYO7A-positive and PROX1-positive cells, respectively.

Experimental design and statistical analysis. For all statistical analyses, at least three samples from each experimental group were analyzed. Student's *t* test was used to determine the differences between two experimental groups. One-way or two-way analysis of variance was performed to assess the differences between more than two experimental groups, and p values <0.05 were considered statistically significant. Statistical analyses were performed using R version 4.2.2 (2022-10-31). All details of statistical analyses are provided in the figures and legends.

Results

Ebf1 is expressed in developing mouse inner ears

In silico analysis of embryonic inner ear epithelia suggested that *Ebf1* is predominantly expressed in the inner ear sensory epithelium during early development (Yamamoto et al., 2021). To quantify *Ebf1* expression at each stage of inner ear development, we performed quantitative reverse transcription polymerase chain reaction (qRT-PCR) using whole embryonic inner ears from E9.5 to P0 (Fig. 1*A*; $F_{(8,18)} = 5.39$; $p = 0.001$; one-way ANOVA with Tukey–Kramer post hoc test). The expression of *Ebf1* mRNA transcripts began to increase at E10.5 and reached a maximum at E13.5 (Fig. 1*A*; $p = 0.00108$). The relative expression level at E13.5 was ∼10-fold higher than that at E9.5. The expression level then decreased but remained 7.5 times higher than that at E9.5 even at P0 (Fig. 1*A*; $p = 0.0154$).

To describe the spatiotemporal expression patterns of *Ebf1* during inner ear development, we performed ISH (Fig. 1*B*,*C*) and IHC (Fig. 2*A*) analyses on sections of the developing inner ear of wild-type mice at various embryonic stages. We stained *Sox2*, which is expressed in the sensory progenitor region of the inner ear from the early developmental stages (Kiernan et al., 2005), as well as *Ebf1* on adjacent sections to specify the location of *Ebf1* expression, and compared the expression of the two genes and their products.

First, we examined *Ebf1* expression at E13.5 (Fig. 1*B*), which is when the sensory epithelium of the inner ear forms and *Ebf1* expression level is maximized during inner ear development (Fig. 1*A*). *Ebf1* was expressed on the medial side of the cochlear duct floor, including the prosensory domain (Fig. 1*B*, white arrows), spiral ganglion (Fig. 1*B*, white asterisks), otic mesenchyme (Fig. 1*B*, black asterisks), and parts of the prosensory regions of the vestibule and crista (Fig. 1*B*, black arrows). Compared with *Sox2*, *Ebf1* was expressed more medially within the cochlear duct floor, which developed into Kölliker's organ and the organ of Corti, and its expression in the vestibule was more restricted (Fig. 1*B*).

Subsequently, we examined the spatiotemporal expression of *Ebf1* throughout inner ear development, including the onset of expression in the inner ear epithelium, using inner ear sections from E9.5 to P0 (Fig. 1*C*). At E9.5, *Ebf1* was not expressed in the otocyst but was expressed in the progenitor cells of the cochleovestibular ganglion (CVG; Fig. 1*C*, white asterisk; E9.5), which delaminate from the ventral side of the otocyst into the otic mesenchyme (Wu and Kelley, 2012). At E10.5, *Ebf1* expression was observed on the ventromedial side of the otocyst, which develops into the cochlear duct, and in the ventrolateral epithelium of the otocyst, which develops into the crista (Fig. 1*C*, black arrowheads; E10.5). Additionally, *Ebf1* expression was detected in the otic mesenchyme (Fig. 1*C*, black asterisk; E10.5) and CVG (Fig. 1*C*, white asterisk; E10.5), which persisted until later stages (Fig. 1*C*). *Ebf1* was expressed in the border region, where the cochlear duct begins to elongate, at E11.5 (Fig. 1*C*, white arrow; E11.5), in the medial side of the cochlear duct floor at E12.5 (Fig. 1*C*, white arrow; E12.5), and in the future crista region in the vestibule at E11.5 and 12.5 (Fig. 1*C*, black arrows; E11.5 and E12.5). In the cochlea at E16.5 and E18.5, *Ebf1* was expressed throughout the organ of Corti and Kölliker's organ (Fig. 1*C*; E16.5 and E18.5), whereas *Sox2* was expressed in the organ of Corti and the lateral half of Kölliker's organ (Fig. 1*C*; E16.5 and E18.5), consistent with a previous report (Urness et al., 2015). *Ebf1* was expressed in the spiral ligaments, tympanic border cells (Fig. 1*C*, white arrowheads; E18.5; Taniguchi et al., 2012), vestibules, and crista (Fig. 1*C*; E18.5). *Ebf1* expression was maintained until P0 (Fig. 1*C*; P0).

IHC analysis showed that EBF1 was expressed throughout Kölliker's organ and the prosensory domain, whereas SOX2 was expressed in a part of Kölliker's organ and the prosensory domain (Fig. 2*A*, top panels), which is consistent with the ISH results. The disappearance of the EBF1 signal from the cochlear epithelia and mesenchyme in conventional *Ebf1* knock-out ($Ebf1^{-/-}$) mice confirmed the specificity of the anti-EBF1 antibody used in this study (Fig. 2*A*, bottom panels).

Ebf1 deletion altered the structure of the cochlear duct

Our ISH and IHC analyses, which showed the expression of *Ebf1* and its protein in both the developing inner ear epithelia and mesenchyme, suggest that *Ebf1* is involved in the development of both the inner ear sensory epithelium and otic mesenchyme. We used two mutant mouse strains to examine the roles of *Ebf1* in developing inner ears: an *Ebf1* conventional knock-out ($Ebf1^{-/-}$) mouse (Lin and Grosschedl, 1995) and a Foxg1-Cre–mediated inner ear epithelia-specific conditional knock-out mouse ($Foxg1Cre;Ebf1^{fl/fl}$; Hébert and McConnell, 2000; Gyory et al., 2012) in which *Ebf1* expression persists in the inner ear mesenchyme (Fig. 2*B*, arrows).

Comparison of the gross morphology of the membranous labyrinth of the inner ear at E18.5 revealed no difference between $Ebf1^{+/+}$ and $Ebf1^{-/-}$ mice (Fig. 3*A*). However, after removing the lateral wall and Reissner's membrane of the cochlea to expose the cochlear duct floor, we found that $Ebf1^{-/-}$ mice had a shorter cochlear duct than $Ebf1^{+/+}$ mice (Fig. 3*B*, white arrowhead).

H&E staining of the cochlea at E18.5 revealed incomplete formation of the scala tympani, particularly in the middle and apical regions of the cochlea of $Ebf1^{-/-}$ mice compared with those of control mice (Fig. 3*C*, arrowheads). Moreover, a spiral limbus is hypoplastic in the basal region and aplastic in the other regions of the cochlea in $Ebf1^{-/-}$ mice (Fig. 3*C*, sl); a lower number of cochlear turns was also observed in the cochlear sections of these mice (Fig. 3*C*, arrows, top right panels), supporting the gross morphological observations.

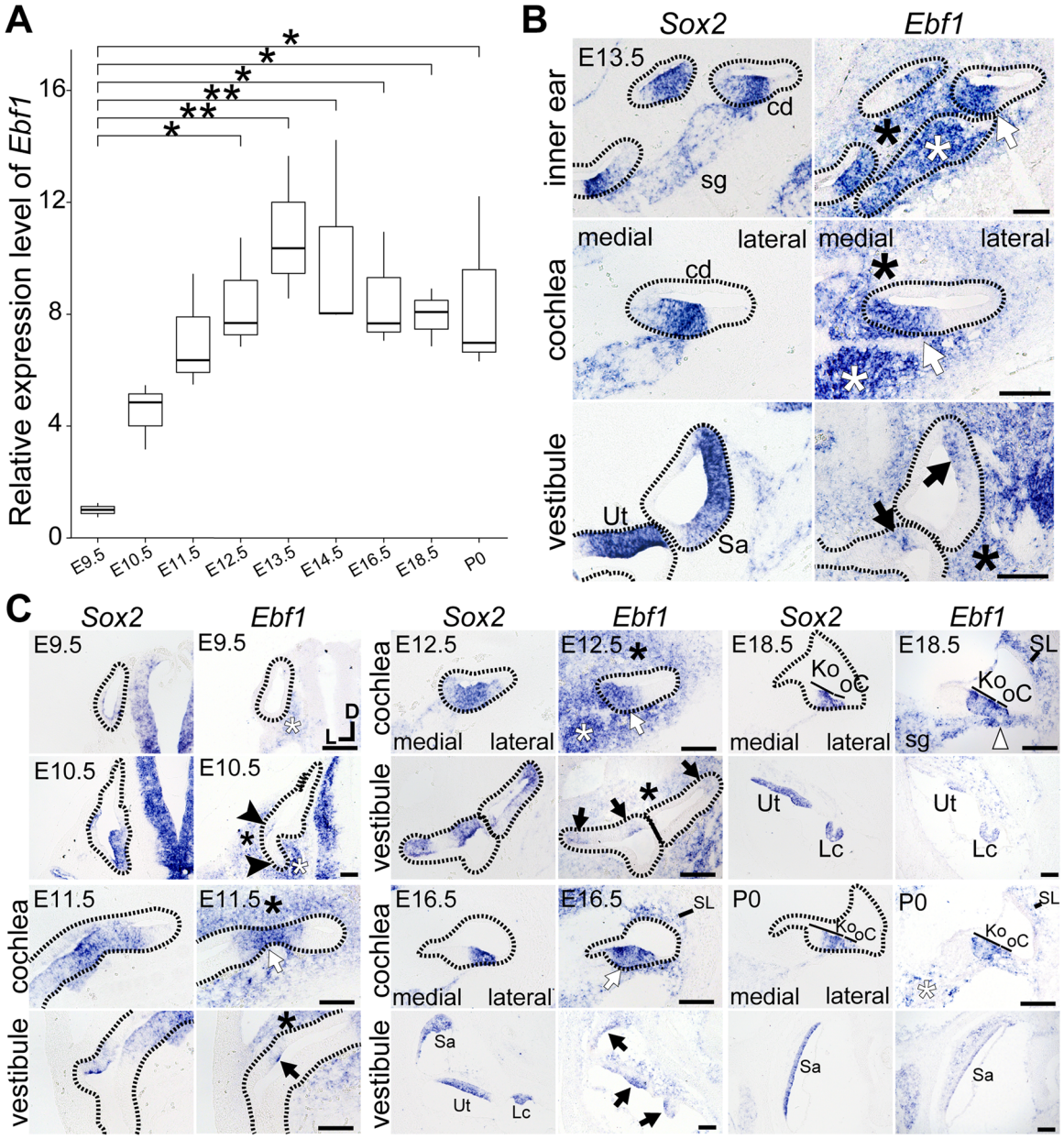

Figure 1. Quantitative and spatiotemporal expression of *Ebf1* during inner ear development. ***A***, Results of qRT-PCR analysis for *Ebf1* in the inner ear of wild-type mice from E9.5 to P0. The value of each date is normalized to the value of E9.5. Box plot representing the medians and interquartile ranges of the relative mRNA expression of *Ebf1* ($n = 3$). ***B***, ***C***, Result of ISH for *Ebf1* and *Sox2* in cross-sections of the inner ear of wild-type mice at E13.5 (***B***) and E9.5, E10.5, E11.5, E12.5, E16.5, E18.5, and P0 (***C***). Areas enclosed by dashed lines indicate the inner ear epithelium. Low-magnification images of the cochlear basal turn and vestibule are presented in the top panels of ***B***. High-magnification images of the apical turn of the cochlear duct and vestibules are presented in the middle and bottom panels of ***B***, respectively. Images of E9.5 and E10.5 otocysts and E11.5, E12.5, E16.5, E18.5, and P0 cochleae and vestibules are presented in the top, middle, and bottom images of ***C***, respectively. From E11.5 to P0, *Ebf1* is expressed in the sensory epithelium of the cochlea (white arrows or Ko and oC), the vestibular and semicircular canals (black arrows), the spiral ganglion (white asterisks), and the surrounding mesenchymal tissues (black asterisks and SL). The expression is detected in tympani border cells (white arrowhead). One-way ANOVA with Tukey–Kramer post hoc tests was performed. $^{*}p < 0.05$, $^{**}p < 0.01$. D, dorsal; L, lateral. cd, cochlear duct; sg, spiral ganglion; Ut, utricle; Sa, saccule; Lc, lateral crista; SL, spiral ligament; Ko, Kölliker's organ; oC, organ of Corti. Scale bar, 100 µm.

Ebf1 was expressed in the otic mesenchyme from early to later developmental stages. To elucidate whether the hypoplastic scala tympani, fewer cochlear turns, and lack of spiral limbus were caused by the *Ebf1*-deficient mesenchyme, we examined the cochlear morphology of *Foxg1Cre;Ebf1*$^{fl/fl}$ and *Foxg1Cre;Ebf1*$^{fl/+}$ mice via H&E staining. In contrast to the hypoplastic scala tympani of *Ebf1*$^{-/-}$ mice, the scala tympani of *Foxg1Cre;Ebf1*$^{fl/fl}$ mice was formed in the whole cochlear turns (Fig. 3C, right panels). The number of cochlear turns in *Foxg1Cre;Ebf1*$^{fl/fl}$ mice was similar to that in the control mice (*Foxg1Cre;Ebf1*$^{fl/+}$ mice). However, *Foxg1Cre;Ebf1*$^{fl/fl}$ mice lacked a spiral limbus, as observed in *Ebf1*$^{-/-}$ mice (Fig. 3C). To quantify the area of a spiral limbus, we performed the IHC of FABP7 (Fig. 3D), which is expressed in a spiral limbus (Saino-Saito et al., 2010). The area of a spiral limbus was significantly smaller in basal and middle turns of *Ebf1*$^{-/-}$ and *Foxg1Cre;Ebf1*$^{fl/fl}$ mice compared with their control mice [Fig. 3E; *Ebf1*$^{+/+}$ vs *Ebf1*$^{-/-}$: basal region ($t_{(6)} = 8.92$; $p = 1.10 \times 10^{-4}$), middle region ($t_{(6)} = 16.8$; $p = 2.85 \times 10^{-6}$); *Foxg1Cre;Ebf1*$^{fl/+}$ vs *Foxg1Cre;Ebf1*$^{fl/fl}$: basal region ($t_{(6)} = 11.0$; $p = 3.43 \times 10^{-5}$), middle region ($t_{(6)} = 12.8$; $p = 1.38 \times 10^{-5}$);

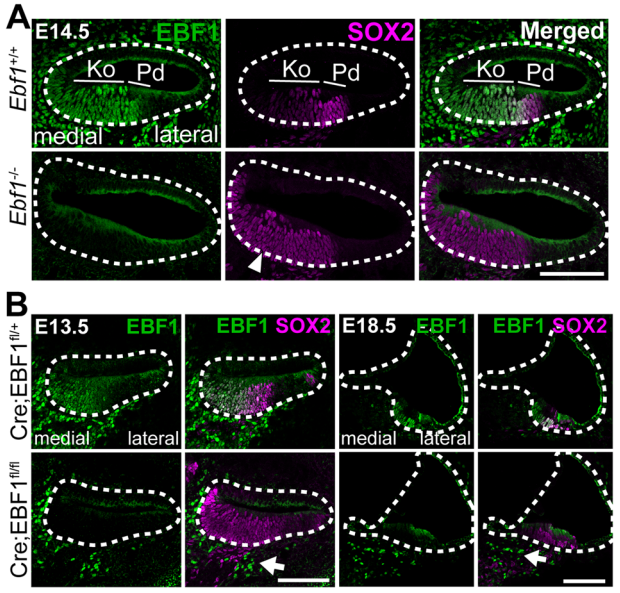

Figure 2. Expression of EBF1 in the cochlea of wild-type and *Ebf1*-deleted mice. ***A***, Immunohistochemical images of E14.5 $Ebf1^{+/+}$ (top panels) and $Ebf1^{-/-}$ (bottom panels) mouse cochlear ducts labeled with EBF1 (green) and SOX2 (magenta). ***B***, Immunohistochemical images of E13.5 (left panels) and E18.5 (right panels) *Foxg1Cre;* $Ebf1^{fl/+}$ (Cre;$EBF1^{fl/+}$; top panels) and *Foxg1Cre;*$Ebf1^{fl/fl}$ (Cre;$EBF1^{fl/fl}$; bottom panels) mouse cochlear ducts labeled with EBF1 (green) and SOX2 (magenta). EBF1 is expressed throughout Kölliker's organ and the prosensory domain, whereas SOX2 was expressed in a part of Kölliker's organ and the prosensory domain as well as otic mesenchyme in wild-type mouse cochlea. The signal for EBF1 is absent in the cochlear epithelium and otic mesenchyme in $Ebf1^{-/-}$ mice and in the cochlear epithelium in *Foxg1Cre;*$Ebf1^{fl/fl}$ mice. The EBF1 signal is observed in the otic mesenchyme of *Foxg1Cre;*$Ebf1^{fl/fl}$ mice (arrows in ***B***). SOX2 is expressed in the medial region of $Ebf1^{-/-}$ mice cochlear duct floor (arrowhead in ***A***). Areas enclosed by dashed lines indicate the cochlear epithelium. Ko, Kölliker's organ; Pd, prosensory domain. Scale bar, 100 µm.

Student's *t* test]. These results suggest that epithelial *Ebf1* does not control the formation of scala tympani and cochlear turns, but mesenchymal *Ebf1* may play a role. In contrast, EBF1 within the epithelia is somehow involved in the spiral limbus formation.

Ebf1 deletion caused an increase in the number of cochlear hair, supporting, and Kölliker's organ cells

Observation of the cochlear epithelia in H&E-stained samples revealed that both $Ebf1^{-/-}$ and *Foxg1Cre;*$Ebf1^{fl/fl}$ mice had deformed Kölliker's organs and organs of Corti (Fig. 3*C*, Ko and oC). To examine these phenotypes more comprehensively, we performed IHC analysis on inner ear sections and cochlear whole-mount samples from E18.5 (Fig. 4).

IHC analysis of cochlear sections showed that *Ebf1* deletion increased the number of MYO7A-positive hair cells as well as SOX2-positive supporting and Kölliker's organ cells from the basal to the apical region at E18.5 in both $Ebf1^{-/-}$ and *Foxg1Cre;*$Ebf1^{fl/fl}$ mice (Fig. 4*A*). An increase in the number of SOX2-positive cells within the medial region of the cochlear duct floor was also observed at E14.5 (Fig. 2*A*, arrowhead). In contrast, *Ebf1* deletion had no morphological effects on the vestibular sensory epithelium (data not shown). Additionally, the apical region of $Ebf1^{-/-}$ mouse cochleae contained multiple layers of SOX2-positive cells (Fig. 4*A*, asterisk). IHC analysis of whole-mount cochlear samples showed that $Ebf1^{-/-}$ and *Foxg1Cre;* $Ebf1^{fl/fl}$ mice had an increased number of MYO7A-positive hair cells (Fig. 4*B*) and ectopic MYO7A-positive cells within the GER (Fig. 4*B*, arrows). Although the normal cochlea has one and three rows of inner and outer hair cells, respectively, the mutant cochlea had eight to nine rows of hair cells. We found ectopic hair cells in seven of the 12 examined $Ebf1^{fl/fl}$ mice cochleae. These ectopic MYO7A-positive cells contained stereocilia-like structures, as indicated by phalloidin staining (Fig. 4*C*, arrows). Increased numbers of supporting cells were confirmed in whole-mount cochlear samples by IHC staining of SOX2 (Fig. 4*B*), a supporting and Kölliker's organ cell marker, and PROX1 (Fig. 4*D*), a pillar and Deiters' cell marker (Bermingham-McDonogh et al., 2006).

To quantify the number of hair and supporting cells, we counted the cells in three regions within the cochlea (basal, middle, and apical regions; Fig. 5*A*) and measured the number of MYO7A- or PROX1-positive cells per 200 µm or all cells within the whole cochlea in $Ebf1^{fl/fl}$ mice and control mice at E18.5. For SOX2-positive cells, we counted the cell number per 100 µm only in the basal regions at E18.5. The results showed that the cochlear hair cell number was significantly increased in $Ebf1^{-/-}$ mice compared with that in $Ebf1^{+/+}$ mice in all three regions (Fig. 5*B*) and the whole cochleae (Fig. 5*C*). $Ebf1^{+/-}$ mice exhibited a significantly higher number of cochlear hair cells than $Ebf1^{+/+}$ mice in the middle and apical regions (Fig. 5*B*; $F_{(4,27)} = 9.43$; $p = 6.64 \times 10^{-5}$; two-way ANOVA with Bonferroni's post hoc test). The hair cell numbers per 200 µm of $Ebf1^{+/+}$, $Ebf1^{+/-}$, and $Ebf1^{-/-}$ mice were 142.3 ± 9.0, 150.0 ± 2.8, and 367.5 ± 30.8 in the basal regions ($Ebf1^{+/+}$ vs $Ebf1^{+/-}$: $p = 1.0$; $Ebf1^{+/+}$ vs $Ebf1^{-/-}$: $p = 3.17 \times 10^{-17}$; $Ebf1^{+/-}$ vs $Ebf1^{-/-}$: $p = 7.69 \times 10^{-17}$); 152.8 ± 8.1, 190.3 ± 7.0, and 363.0 ± 22.4 in the middle regions ($Ebf1^{+/+}$ vs $Ebf1^{+/-}$: $p = 7.67 \times 10^{-3}$; $Ebf1^{+/+}$ vs $Ebf1^{-/-}$: $p = 1.81 \times 10^{-16}$; $Ebf1^{+/-}$ vs $Ebf1^{-/-}$: $p = 2.33 \times 10^{-14}$); and 154.5 ± 5.1, 183.5 ± 6.8, and 440.3 ± 23.8 in the apical regions ($Ebf1^{+/+}$ vs $Ebf1^{+/-}$: $p = 4.79 \times 10^{-2}$; $Ebf1^{+/+}$ vs $Ebf1^{-/-}$: $p = 7.07 \times 10^{-20}$; $Ebf1^{+/-}$ vs $Ebf1^{-/-}$: $p = 1.12 \times 10^{-18}$), respectively. The numbers of $Ebf1^{+/+}$ and $Ebf1^{-/-}$ hair cells in the whole cochlea were 2,559.3 ± 108.0 and 4,302.0 ± 194.2, respectively (Fig. 5*C*; $t_{(4)} = -11.1$; $p = 3.76 \times 10^{-4}$; Student's *t* test).

SOX2-positive cells, constituting a part of Kölliker's organ cells and supporting cells within organs of Corti, also increased in number by 1.7 times in $Ebf1^{-/-}$ mice compared with those in $Ebf1^{+/+}$ mice (Fig. 5*D*; $t_{(6)} = -16.5$; $p = 3.19 \times 10^{-6}$; Student's *t* test). PROX1-positive cell numbers significantly increased in $Ebf1^{-/-}$ mice compared with those in $Ebf1^{+/+}$ mice only in the basal and middle regions (Fig. 5*E*; $F_{(2,18)} = 91.41$; $p = 3.73 \times 10^{-10}$; two-way ANOVA with Bonferroni's post hoc test). In the apical region, the number of PROX1-positive cells was similar to that in $Ebf1^{-/-}$ and $Ebf1^{+/+}$ mice. The numbers of PROX1-positive cells in $Ebf1^{+/+}$ and $Ebf1^{-/-}$ mice were 203.3 ± 2.2 and 439.0 ± 15.4, 228.0 ± 16.8 and 389.8 ± 10.4, and 196.0 ± 27.3 and 204.5 ± 19.6 in the basal, middle, and apical regions, respectively (Fig. 5*E*; basal, $p = 1.56 \times 10^{-13}$; middle, $p = 8.99 \times 10^{-11}$; apical, $p = 0.492$). When comparing the PROX1-positive cell numbers in the whole cochlea, the number was significantly higher in $Ebf1^{-/-}$ mice (4,980.7 ± 84.6) than that in $Ebf1^{+/+}$ mice (3,769.7 ± 89.4; Fig. 5*F*; $t_{(4)} = -13.9$; $p = 1.54 \times 10^{-4}$; Student's *t* test).

We performed IHC analysis using more specific markers to reveal which population of hair or supporting cells increased in number in $Ebf1^{-/-}$ mice (Fig. 6). We immunostained whole-mounted cochlea at E18.5 with anti-VGLUT3 and anti-p75 (NGFR) antibodies, which indicate inner hair (Li et al., 2018) and pillar cells (von Bartheld et al., 1991), respectively. VGLUT3-positive inner hair cells, which are arranged in a single row in wild-type mice, were found to be increased in number in $Ebf1^{-/-}$ mice (Fig. 6*A*), indicating an increase in both inner

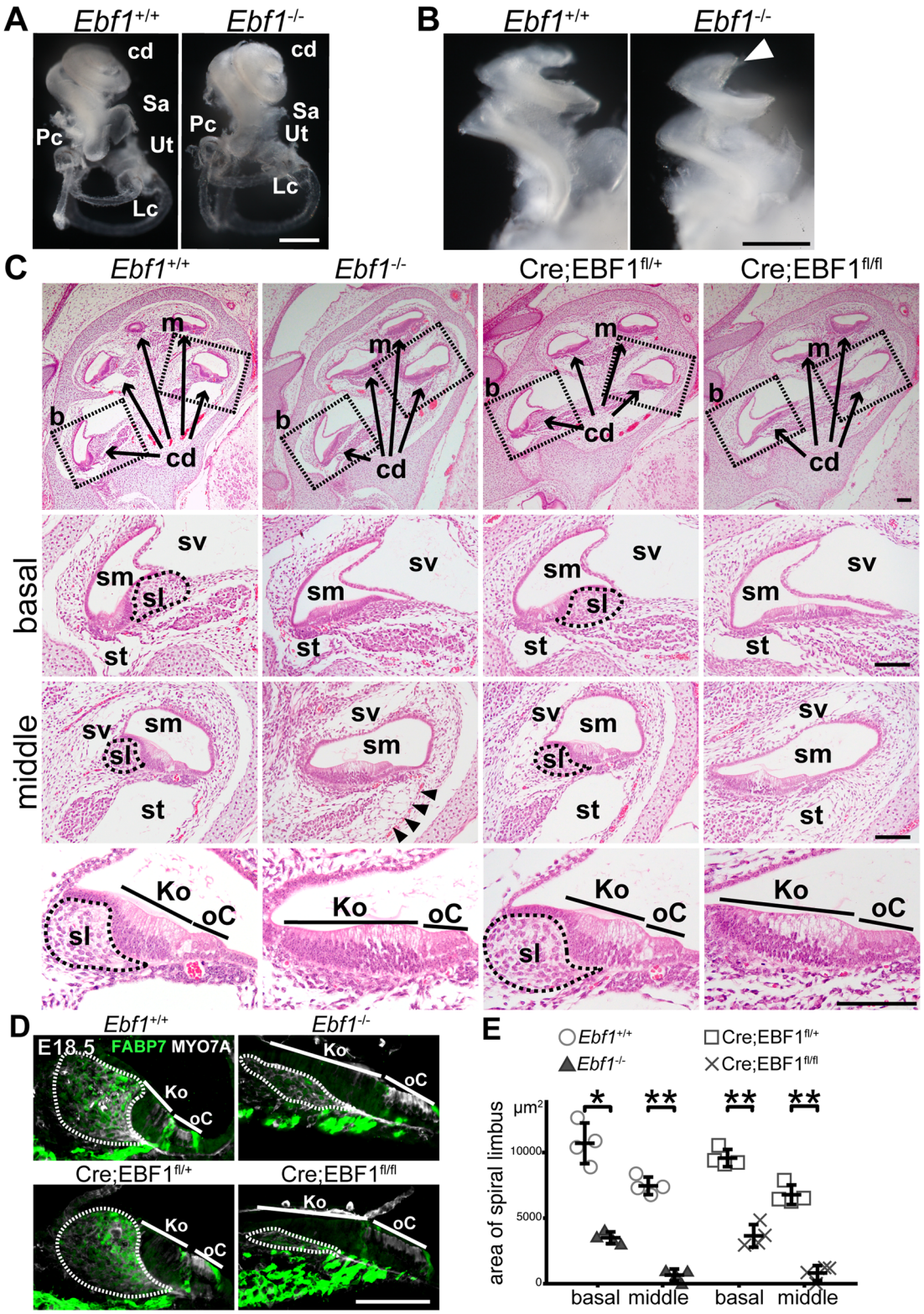

Figure 3. Development of the cochlear duct is deteriorated in *Ebf1*-deleted mice. ***A***, Gross morphology of membranous labyrinth of the inner ear of *Ebf1*$^{+/+}$ and *Ebf1*$^{-/-}$mice at E18.5. ***B***, Gross morphology of the cochlear duct floor after the lateral wall and Reissner's membrane of the cochlea were removed at E18.5. ***C***, H&E-stained cross-sections of the cochlea at E18.5 from *Ebf1*$^{+/+}$, *Ebf1*$^{-/-}$, *Foxg1Cre;Ebf1*$^{fl/+}$ (Cre;EBF1$^{fl/+}$), and *Foxg1Cre;Ebf1*$^{fl/fl}$ (Cre;EBF1$^{fl/fl}$) mice. Images in dashed boxes in the top row were magnified into the second row (from boxes labeled as b in the top row, a basal turn) and the third row (from boxes labeled as m in the top row, a middle turn). The images in the bottom row are the magnified images of the third row (middle turn). Areas enclosed by dashed lines indicate the spiral limbus. ***D***, Immunohistochemical images of the basal turn of the *Ebf1*$^{+/+}$, *Ebf1*$^{-/-}$, *Foxg1Cre;Ebf1*$^{fl/+}$, and *Foxg1Cre;Ebf1*$^{fl/fl}$ mice cochlear ducts at E18.5, labeled with MYO7A (gray) and FABP7 (green). Areas enclosed by dashed lines indicate the spiral limbus. ***E***, Areas of spiral limbus in the basal and middle region of the cochlear ducts of *Ebf1*$^{+/+}$, *Ebf1*$^{-/-}$, *Foxg1Cre;Ebf1*$^{fl/+}$, and *Foxg1Cre;Ebf1*$^{fl/fl}$ mice at E18.5. Student's *t* test was performed for comparison between *Ebf1*-deleted mice (*Ebf1*$^{-/-}$ or *Foxg1Cre;Ebf1*$^{fl/fl}$) and respective controls (*Ebf1*$^{+/+}$ or *Foxg1Cre;Ebf1*$^{fl/+}$). *$p < 0.001$, **$p < 0.0001$. Error bars represent mean ± standard deviation ($n = 4$). cd, cochlear duct; Ut, utricle; Sa, saccule; Lc, lateral crista; Pc, posterior crista; b, basal turn; m, middle turn; sv, scala vestibuli; sm, scala media; st, scala tympani; sl, spiral limbus: Ko, Kölliker's organ; oC, organ of Corti. Scale bars: ***A***, ***B***, 0.5 mm; ***C***, ***D***, 100 μm.

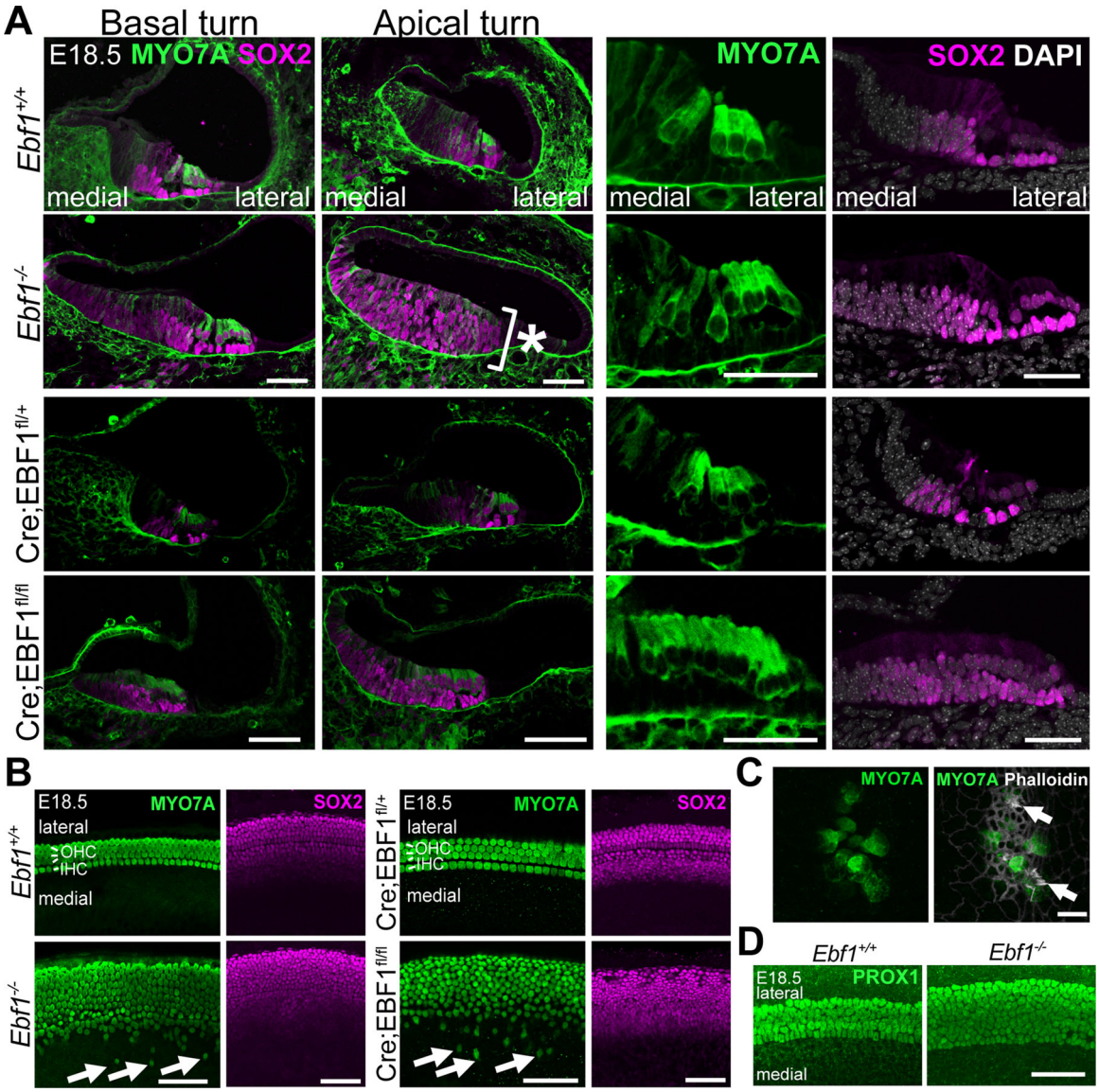

Figure 4. *Ebf1* deletion increases the number of MYO7A-, SOX2-, and PROX1-positive cells in the cochlea. ***A***, Cross-sections of the basal and apical turns of the cochlea of *Ebf1*$^{+/+}$, *Ebf1*$^{-/-}$, *Foxg1Cre;Ebf1*$^{fl/+}$ (Cre;EBF1$^{fl/+}$), and *Foxg1Cre;Ebf1*$^{fl/fl}$ (Cre;EBF1$^{fl/fl}$) mice at E18.5, labeled with MYO7A (green) and SOX2 (magenta). Magnified images of the organ of Corti (oC) and Kölliker's organ (Ko) are presented in the eight right panels. ***B***, Whole-mount cochlear images from *Ebf1*$^{+/+}$, *Ebf1*$^{-/-}$, *Foxg1Cre;Ebf1*$^{fl/+}$ (Cre;EBF1$^{fl/+}$), and *Foxg1Cre;Ebf1*$^{fl/fl}$ (Cre;EBF1$^{fl/fl}$) mice, labeled with MYO7A (green) and SOX2 (magenta). ***C***, ***D***. Whole-mount cochlear images from *Ebf1*$^{+/+}$ and *Ebf1*$^{-/-}$ mice at E18.5, labeled with MYO7A (green, ***C***), phalloidin (white, ***C***), and PROX1 (green, ***D***). Scale bars: ***A***, ***B***, ***D***, 50 µm; ***C***, 10 µm.

and outer hair cells. The number of p75-positive pillar cells, which separate inner and outer hair cells, did not increase in *Ebf1*$^{-/-}$ mice (Fig. 6*B*). Considering that PROX1-positive cells indicate pillar and Deiters' cells, the number of Deiters' cells increased in *Ebf1*$^{-/-}$ mice. However, the arrangement of pillar cells was disrupted in *Ebf1*$^{-/-}$ mice (Fig. 6*B*, arrows), which was reflected in the appearance of VGLUT3 cells in the outer hair cell region of *Ebf1*$^{-/-}$ mice (Fig. 6*A*, arrowheads). In *Ebf1*$^{-/-}$ mice, the maturation markers, VGLUT3 and p75, were detected only in part of the cochlear regions. VGLUT3 was detected only in the basal region and p75 was in the basal and middle regions.

The total cochlear length, measured based on the length of the MYO7A-positive region (Fig. 7*A*), was slightly, but significantly, shorter in *Ebf1*$^{-/-}$ mice than that in *Ebf1*$^{+/+}$ and *Ebf1*$^{+/-}$ mice (Fig. 7*B*; $F_{(2,15)} = 21.03$; $p = 4.44 \times 10^{-5}$; one-way ANOVA with Tukey–Kramer post hoc test; *Ebf1*$^{+/+}$ vs *Ebf1*$^{+/-}$: $p = 0.779$; *Ebf1*$^{+/+}$ vs *Ebf1*$^{-/-}$: $p = 2.74 \times 10^{-4}$; *Ebf1*$^{+/-}$ vs *Ebf1*$^{-/-}$: $p = 7.80 \times 10^{-5}$).

Ebf1 deletion caused the aberrant spiral ganglion and nerve fibers

As *Ebf1* is expressed in the spiral ganglion and the number of hair cells, a target of the spiral ganglion cell axon, increased in *Ebf1*$^{-/-}$ mice, we examined the spiral ganglion morphology and innervation of cochlear hair cells with IHC using anti-Tubulin β 3 (TUJ1) antibodies at E18.5 (Fig. 8).

Compared with *Ebf1*$^{+/+}$ mice, which exhibited axons extending from the spiral ganglion cells to the cochlear hair cells, *Ebf1*$^{-/-}$ mice had spiral ganglion cells (Fig. 8*A*, sg) under the organs of Corti (Fig. 8*A*, arrows), as well as in their normal position. The axons, which usually run parallel to the rows of outer hair cells, formed a reticulation within the *Ebf1*$^{-/-}$ mouse cochlear hair

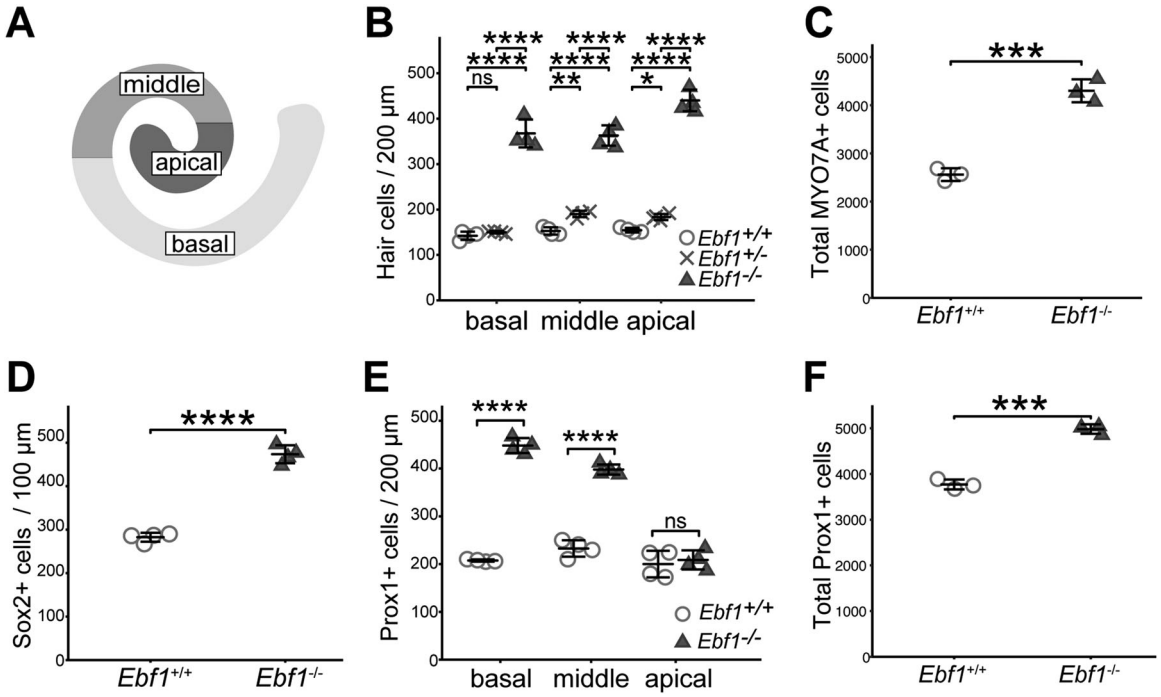

Figure 5. Increases in the number of hair and supporting cells. ***A***, Schematic diagram of the cochlea duct showing the positions of the basal, middle, and apical regions of the cochlea. ***B***, Total hair cell numbers per 200 µm in the basal, middle, and apical regions of the cochlear ducts of $Ebf1^{+/+}$, $Ebf1^{+/-}$, and $Ebf1^{-/-}$ mice at E18.5. ***C***, Numbers of MYO7A-positive cells per total cochlear length. ***D***, Numbers of SOX2-positive cells per 100 µm in the basal region of the cochlea. ***E***, Numbers of PROX1-positive cells per 200 µm in the basal, middle, and apical regions of the cochlea. ***F***, Numbers of PROX1-positive cells per total cochlear length. Two-way ANOVA with Bonferroni's post hoc test (***B***, ***E***) and Student's *t* test (***C***, ***D***, ***F***) were performed. $*p < 0.05$, $**p < 0.01$, $***p < 0.001$, and $****p < 0.0001$; ns, not significant. Error bars represent mean ± standard deviation ($n = 4$ for ***B***, ***D***, ***E*** and $n = 3$ for ***C***, ***F***).

cell regions (Fig. 8*B*,*C*). Moreover, the innervation reached Kölliker's organ (Fig. 8*A*, arrowheads and brackets) as well as the organ of Corti.

Ebf1 deletion changed the distribution of JAG1-positive Kölliker's organ cells, the differentiation timing of a prosensory domain, and the proliferation of SOX2-positive cells

As $Ebf1^{-/-}$ mice had increased numbers of cochlear hair cells, which were differentiated from the prosensory domain, we investigated its specification, differentiation, proliferation, and cell death in the $Ebf1^{-/-}$ mouse cochlear duct floor.

First, to determine whether the formation of the prosensory domain was affected by *Ebf1* deletion, we examined the formation of regions medial and lateral to the prosensory domain. Because these regions express FGF10 and BMP4 to induce nonsensory or sensory epithelia in the cochlear duct floor (Ohyama et al., 2010; Urness et al., 2015), respectively, we performed ISH for *Fgf10* and *Bmp4* in the basal region of the cochlear duct of $Ebf1^{+/+}$ *and* $Ebf1^{-/-}$ mice at E13.5 (Fig. 9*A*). The formation of both regions was similar in $Ebf1^{+/+}$ and $Ebf1^{-/-}$ mice, suggesting that *Ebf1* is not involved in the development of cell populations expressing *Fgf10* or *Bmp4*. To verify the medial cell population more precisely, we immunostained E13.5 and E14.5 cochleae with an anti-JAG1 antibody (Fig. 9*A*), as JAG1 is exclusively expressed in Kölliker's organ, a part of the medial region, at this stage (Ohyama et al., 2010). JAG1-positive cells in $Ebf1^{-/-}$ mouse cochlea expanded to the more medial region compared with those in $Ebf1^{+/+}$ mouse cochlea at E13.5 and E14.5 (Fig. 9*A*, arrowheads).

Subsequently, we examined the expression of *Atoh1* within the prosensory domain via ISH at E14.5 and E15.5 (Fig. 9*B*), as *Atoh1* is necessary for hair cells to differentiate from the prosensory cell population (Bermingham et al., 1999) and its expression indicates the initiation of hair cell development from the prosensory domain. Compared with $Ebf1^{+/+}$ mice that expressed *Atoh1* within the prosensory domain from E14.5, *Atoh1* mRNA was not detected in the basal to middle region of the E14.5 $Ebf1^{-/-}$ mouse cochlea, although the vestibular organs expressed *Atoh1* within the prosensory epithelia. However, E15.5 $Ebf1^{-/-}$ mice exhibited an *Atoh1* signal within the prosensory domain of the cochlea. This result suggests that while the cell fate specification of sensory epithelia in the cochlea is not affected, its timing is delayed by *Ebf1* deletion. Considering that the differentiation of cochlear sensory epithelia promotes the transition from the basal to apical turns of the cochlea (Sher, 1971), the expression of hair and supporting cell markers at a later stage, E18.5, also indicated delayed differentiation of $Ebf1^{-/-}$ mouse cochleae (Fig. 6). These markers were found to be detected in more basal cochlear regions in $Ebf1^{-/-}$ mice than those in $Ebf1^{+/+}$ mice.

The expansion of the JAG1-positive cell area and the increased numbers of hair and supporting cells suggest that the enhancement of proliferation or suppression of cell death occurs within the prosensory domain and Kölliker's organ of $Ebf1^{-/-}$ mouse cochlea. To identify the mechanisms that correlate with the functions of EBF1 within the cochlea, we tested the proliferation and apoptotic status of $Ebf1^{-/-}$ mouse cochlea. To evaluate the proliferation status of the prosensory domain and Kölliker's organ, we immunostained cochlear sections with SOX2, a marker of the prosensory domain and a part of Kölliker's organ, and 5-ethynyl-2′-deoxyuridine (EdU) at E12.5, 13.5, 14.5, and 16.5 after administering EdU to pregnant mice (Fig. 10*A*). Quantification of SOX2-positive cells showed that their number decreased in $Ebf1^{+/+}$ mice from E12.5 onward (Fig. 10*B*), and their location was limited to the prosensory

domain (Fig. 10A, brackets). In contrast, SOX2-positive cells in *Ebf1*$^{-/-}$ mouse cochlea were found both in the prosensory domain and the medial region, even at E13.5, which was consistent with the results of JAG1 immunostaining (Fig. 9A). The number of SOX2-positive cells in *Ebf1*$^{-/-}$ mice was similar to that in *Ebf1*$^{+/+}$ mice at E12.5 but increased at E13.5 and returned to the E12.5 level at E14.5 (Fig. 10B). Therefore, the number of SOX2-positive cells in *Ebf1*$^{-/-}$ mice was significantly higher than that in *Ebf1*$^{+/+}$ mice at E13.5 and E14.5 (Fig. 10B; $F_{(2,18)} = 12.61$; $p = 3.80 \times 10^{-4}$; two-way ANOVA with Bonferroni's post hoc test; $p = 2.49 \times 10^{-4}$ for E13.5 and $p = 1.36 \times 10^{-5}$ for E14.5). The number of EdU-positive proliferating cells within SOX2-positive cells was significantly higher in *Ebf1*$^{-/-}$ mice than that in *Ebf1*$^{+/+}$ mice at E13.5 and E14.5 (Fig. 10C; $F_{(2,18)} = 10.61$; $p = 9.50 \times 10^{-4}$; two-way ANOVA with Bonferroni's post hoc test; $p = 9.55 \times 10^{-6}$ for E13.5 and $p = 1.00 \times 10^{-3}$ for E14.5). As the number of SOX2-positive cells increased in *Ebf1*$^{-/-}$ mice after E13.5 (Fig. 10B), normalization of SOX2-positive cell numbers was necessary to correctly evaluate the proliferation status of SOX2-positive cells. We calculated the proportion of EdU-positive cells among SOX2-positive cells and found that the proliferation was enhanced in the SOX2-positive cells of *Ebf1*$^{-/-}$ mouse cochlea only at E13.5 (49.8 ± 4.3%) compared with that in *Ebf1*$^{+/+}$ mouse cochlea (37.8 ± 4.2%; Fig. 10D; $F_{(2,18)} = 5.84$; $p = 0.011$; two-way ANOVA with Bonferroni's post hoc test; $p = 9.45 \times 10^{-4}$ for E13.5). These results suggested that EBF1 suppressed the proliferation of SOX2-positive cells within a limited time window. Morphologically, a difference in proliferation was observed in the prosensory domain, as indicated by EdU immunostaining (Fig. 10A, brackets at E13.5). EdU staining was observed in the Kölliker's organs of *Ebf1*$^{-/-}$ mice, even at E16.5 (Fig. 10A, arrowhead) but not observed in *Ebf1*$^{+/+}$ mice (Fig. 10A, E16.5).

The loss of proliferation within the prosensory domain ~E13.5 (Fig. 10A, bracket in the *Ebf1*$^{+/+}$ sample at E13.5) has been well documented in previous studies (Chen and Segil, 1999; Chen et al., 2002). The post-mitotic domain is called the zone of nonproliferating cells (ZNPC) and is characterized by the expression of the cyclin-dependent kinase inhibitor CDKN1B. To confirm the EdU immunostaining results, we performed CDKN1B immunostaining at E13.5 and E14.5 (Fig. 10E). Although CDKN1B was detected in the prosensory domain of *Ebf1*$^{+/+}$ mice at E13.5, it was not expressed in *Ebf1*$^{-/-}$ mouse cochlea at this stage (Fig. 10E, arrows), which was consistent with the results of EdU detection. At E14.5, CDKN1B was detected in a larger area of the middle part of *Ebf1*$^{-/-}$ mouse cochlear duct floors than in those of *Ebf1*$^{+/+}$ mice. To quantify the change of the CDKN1B immunostaining, we counted the number of CDKN1B- and SOX2-double-positive cells at E13.5 and E14.5 (Fig. 10F). We found that *Ebf1* deletion resulted in significant loss of CDKN1B- and SOX2-double-positive cells at E13.5 (79.0 ± 3.7; *Ebf1*$^{+/+}$ vs 2.6 ± 2.1; *Ebf1*$^{-/-}$; $t_{(4)} = 25.3$; $p = 1.45 \times 10^{-5}$; Student's *t* test). In contrast, the number in *Ebf1*$^{-/-}$ mice was almost twice as high as that in *Ebf1*$^{+/+}$ mice at E14.5 (43.3 ± 8.7; *Ebf1*$^{+/+}$ vs 87.3 ± 4.8; *Ebf1*$^{-/-}$; $t_{(6)} = -7.68$; $p = 2.54 \times 10^{-4}$; Student's *t* test). Apoptosis within the inner ear or cochlear duct did not increase in *Ebf1*$^{-/-}$ mice at E11.5 and E13.5, compared with that in *Ebf1*$^{+/+}$ mice (Fig. 11).

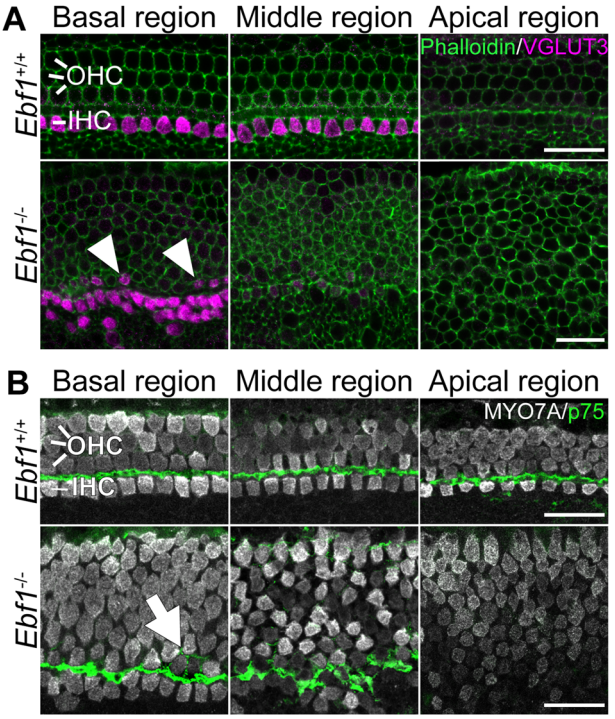

Figure 6. *Ebf1* deletion causes an increased number of inner hair cells and delayed differentiation of hair and supporting cells. High-magnification images of the basal, middle, and apical regions of whole-mount cochlear samples from E18.5 *Ebf1*$^{+/+}$ and *Ebf1*$^{-/-}$ mice. ***A***, Immunostaining with phalloidin (green) and an anti-VGLUT3 antibody (magenta). In the cochlea of *Ebf1*$^{-/-}$ mice, the row number of VGLUT3-positive cells was 2 to 3, whereas this number was only 1 in wild-type mice. VGLUT3-positive cells were observed only in the basal region of the cochlea but not in the middle and apical regions of *Ebf1*$^{-/-}$ mice. Several VGLUT3-positive cells were observed in the outer hair cell area (arrowheads). ***B***, Immunostaining with anti-MYO7A (gray) and p75 (green) antibodies. In the cochlea of *Ebf1*$^{-/-}$ mice, the row number of p75-positive cells was similar to that in *Ebf1*$^{+/+}$ mice, although their arrangement was deteriorated in *Ebf1*$^{-/-}$ mice (arrow). p75-positive cells are observed only in the basal and middle regions in the *Ebf1*$^{-/-}$ mice. Scale bar, 20 µm.

Ebf1 deletion impairs auditory function

The aberrant cochlear sensory epithelia observed in *Ebf1*-deleted mice suggest that hearing ability is impaired in these mice. To

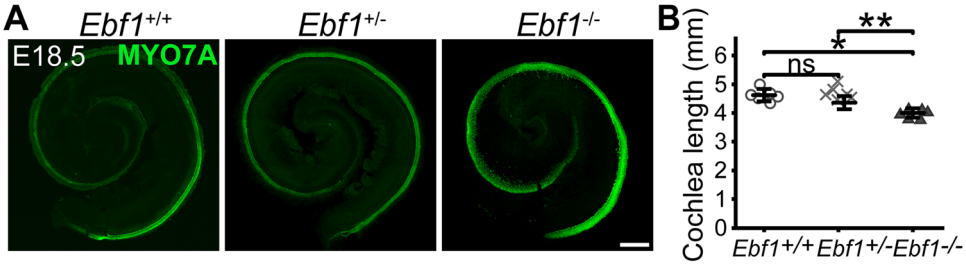

Figure 7. Quantification of cochlear length. ***A***, Whole-mount images of the cochlea of E18.5 *Ebf1*$^{+/+}$, *Ebf1*$^{+/-}$, and *Ebf1*$^{-/-}$ mice labeled with MYO7A (green). ***B***, Quantification of cochlear duct length of E18.5 *Ebf1*$^{+/+}$, *Ebf1*$^{+/-}$, and *Ebf1*$^{-/-}$ mice. The cochlear length of *Ebf1*$^{-/-}$ mice was significantly shorter than that of *Ebf1*$^{+/+}$and *Ebf1*$^{+/-}$ mice. Two-way ANOVA with Bonferroni's post hoc test was performed. *$p < 0.001$, and **$p < 0.0001$; ns, not significant. Error bars represent mean ± standard deviation ($n = 6$). Scale bar, 200 µm.

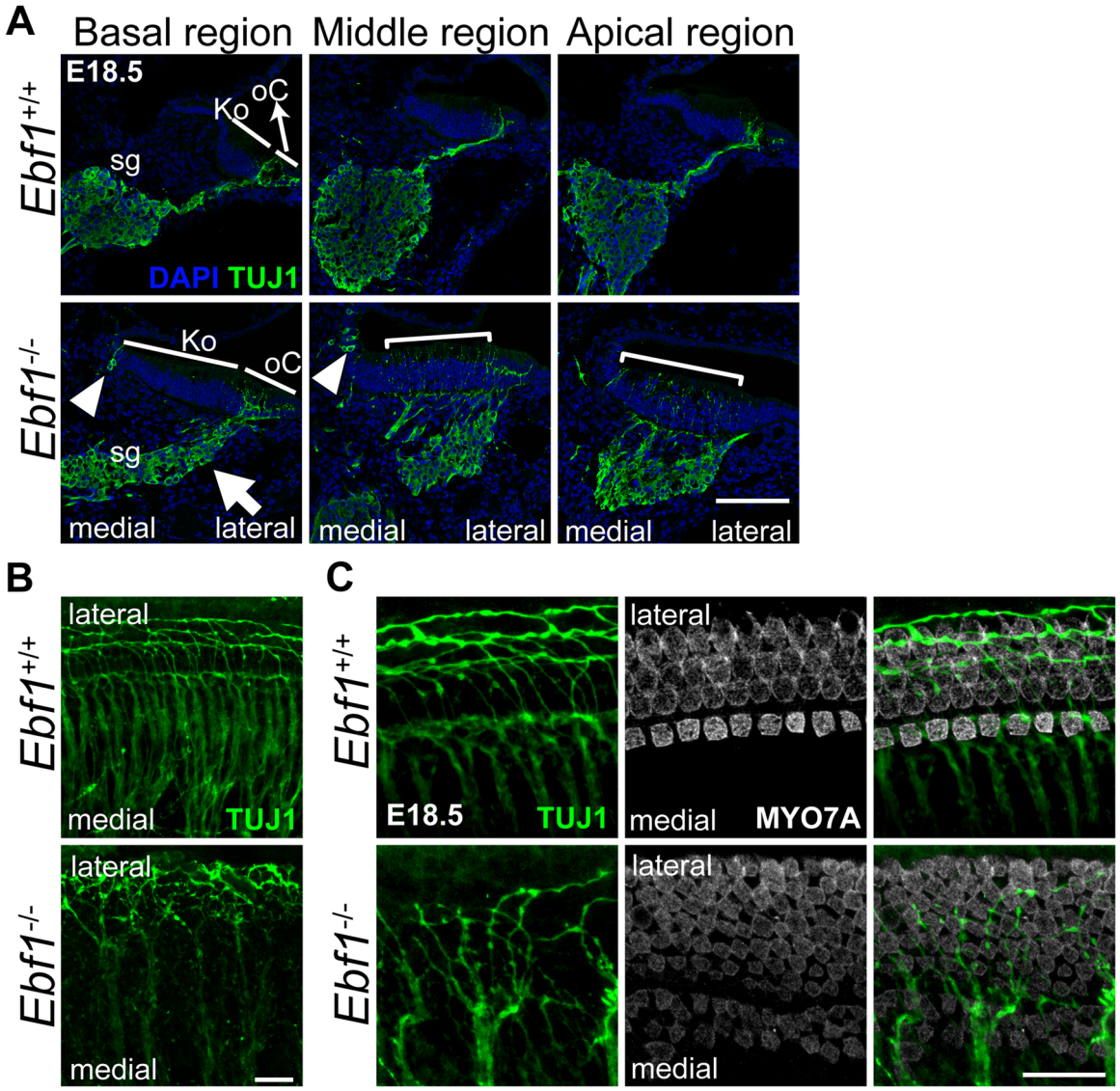

Figure 8. *Ebf1* deletion causes aberrant spiral ganglion development and axon outgrowth to cochlear hair cells. ***A***, Cross-sections of the basal, middle, and apical regions of the cochlea and spiral ganglion in E18.5 $Ebf1^{+/+}$ and $Ebf1^{-/-}$ mice stained with Tubulin β 3 (TUJ1, green) and 4′,6-diamidino-2-phenylindole (DAPI, gray). The morphology of the spiral ganglion in $Ebf1^{-/-}$ mice differed from that in $Ebf1^{+/+}$ mice. TUJ1-positive cell bodies were observed below the organ of Corti (arrow) and at their normal site. Additionally, innervation from the spiral ganglion was observed in the hair cell part and in Kölliker's organ in the middle and apical of the cochlea (arrowheads and brackets). ***B***, Low-magnification view of the basal region of the whole-mount cochlear image in E18.5 $Ebf1^{+/+}$ and $Ebf1^{-/-}$ mice labeled with TUJ1 (green). ***C***, High-magnification view of the basal region of the whole-mount cochlear image in E18.5 $Ebf1^{+/+}$ and $Ebf1^{-/-}$ mice labeled with TUJ1 (green) and MYO7A (gray). In $Ebf1^{+/+}$ mice, the neurons ran parallel to the outer hair cells, whereas, in $Ebf1^{-/-}$ mice, the neurons formed a reticulation within the cochlear hair cell regions. Scale bars: ***A***, 100 µm; ***B***, ***C***, 20 µm.

evaluate the effect of *Ebf1* deletion on auditory function, we measured the ABR (Fig. 12*A*) and DPOAE (Fig. 12*B*) in P21 $Foxg1Cre;Ebf1^{fl/fl}$ mice. We did not use $Ebf1^{-/-}$ mice for this analysis to avoid embryonic lethality and to eliminate the effects of the hypoplastic scala tympani observed in $Ebf1^{-/-}$mice on auditory function. The phenotype of $Foxg1Cre;Ebf1^{fl/fl}$ mice was evaluated using whole-mount cochlear samples collected at P23 (Fig. 12*C*). We observed a marked increase in the number of cochlear hair cells in $Foxg1Cre;Ebf1^{fl/fl}$ mice, comparable to the morphology of E18.5 $Ebf1^{-/-}$ and $Foxg1Cre;Ebf1^{fl/fl}$ mice (Figs 4*B*, 12*C*).

ABR measurement showed significant elevations of thresholds of the response to sound in $Foxg1Cre;Ebf1^{fl/fl}$ mice at all frequencies examined (10 kHz, 93.3 ± 2.5 dB; 20 kHz, 86.7 ± 3.8 dB; 40 kHz, 105.0 ± 0.0 dB; Fig. 12*A*; $F_{(2,12)} = 5.21$; $p = 0.023$; two-way ANOVA with Bonferroni's post hoc test) compared with control mice, indicating severe hearing loss in *Ebf1*-deleted mice. Subsequently, we performed DPOAE tests to assess the function of the increased number of outer hair cells caused by *Ebf1* deletion because DPOAE detects nonlinear responses of outer hair cells to sound. The DPOAE responses in $Foxg1Cre;Ebf1^{fl/fl}$ mice were significantly lower than those in control mice (Fig. 12*B*; $F_{(7,48)} = 5.54$; $p = 1.03 \times 10^{-4}$; two-way ANOVA with Bonferroni's post hoc test). The decreased DPOAE response in $Foxg1Cre;Ebf1^{fl/fl}$ mice also suggests that the increased number of hair cells caused by *Ebf1* deletion did not function as outer hair cells.

Discussion

The results of this study indicate a novel and interesting role of *Ebf1* in the cochlear development. *Ebf1* controls numbers of

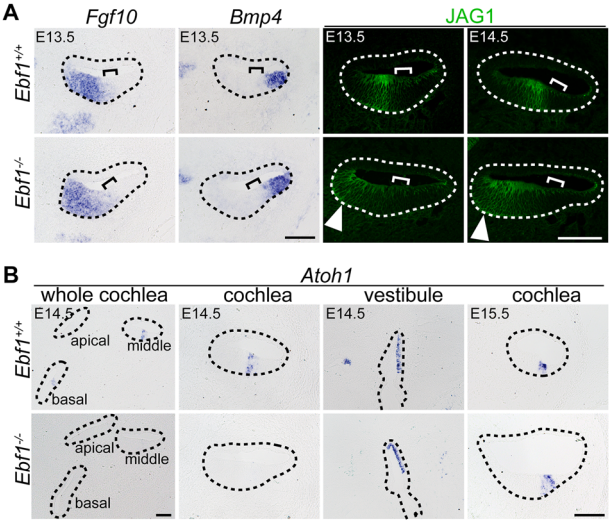

Figure 9. *Ebf1* deletion causes JAG1 expression to spread inward, delaying *Atoh1* expression during cochlear development. ***A***, Results of ISH of *Fgf10* and *Bmp4* and immunostaining of JAG1 (green) on cross-sections of the basal-to-middle region of the cochlea of $Ebf1^{+/+}$ and $Ebf1^{-/-}$ mice at E13.5 and E14.5. The prosensory domain is shown in brackets. ***B***, Result of ISH of *Atoh1* on cross-sections of the basal-to-middle region of the cochlea of $Ebf1^{+/+}$ and $Ebf1^{-/-}$ mice at E14.5 and E15.5. Areas enclosed by dashed lines indicate cochlear ducts and vestibules. Scale bar, 100 µm.

both hair and supporting cells within the cochlear sensory epithelia. Moreover, *Ebf1* is important for the development of the scala tympani, spiral limbus, and spiral ganglion cells.

Since EBF1 was originally identified from the regulators of early B-cell differentiation (Hagman et al., 1991) and olfactory-specific genes (Wang and Reed, 1993), its expression has been reported in all three germinal layers (Liberg et al., 2002). EBF1 has many roles, including cell fate specification, the differentiation, maturation, and migration of cells, and path findings by neurons (Liberg et al., 2002).

The present study revealed that *Ebf1* is expressed in ectodermal tissues (the inner ear epithelium and spiral ganglion) and the otic mesenchymal tissues. Its expression in the inner ear began at approximately E10.5, as confirmed by qRT-PCR and ISH (Fig. 1*A*,*C*). Within the cochlea, *Ebf1* expression in the cochlea was not limited to the *Sox2*-positive prosensory domain (Fig. 1*B*, white arrows) but expanded toward a more medial region in the cochlear duct floor, where Kölliker's organ exists (Figs. 1*B*,*C*, 2*A*). Thus, the *Ebf1* expression area comprised most of the GER.

To elucidate the function of *Ebf1* in inner ear development, we examined the inner ear morphology of *Ebf1* conventional ($Ebf1^{-/-}$) and inner ear epithelia-specific conditional ($Foxg1Cre;Ebf1^{fl/fl}$) knock-out mice. In contrast to the normal vestibular morphology of $Ebf1^{-/-}$ mice, the cochlea of *Ebf1*-deleted mice showed various phenotypes, indicating that other *Ebf* subtypes do not have redundant functions with *Ebf1* in the cochlea as in B-cells, osteoblasts, and the striatum (Lin and Grosschedl, 1995; Garel et al., 1999; Nieminen-Pihala et al., 2021). H&E staining revealed loss of the scala tympani and spiral limbus in $Ebf1^{-/-}$ mice (Fig. 3*C*). Because both structures are derived from mesenchymal tissues (Sher, 1971; Phippard et al., 1999), we hypothesized that these phenotypes reflect the roles of EBF1 in cochlear mesenchyme. To confirm this, we compared the formation of the scala tympani and spiral limbus between $Ebf1^{-/-}$ and $Foxg1Cre;Ebf1^{fl/fl}$ mice (Fig. 3*C*). Although the scala tympani developed normally in $Foxg1Cre;Ebf1^{fl/fl}$ mice, the spiral limbus was hypoplastic in both $Foxg1Cre;Ebf1^{fl/fl}$ and $Ebf1^{-/-}$ mice. These results clearly indicate that EBF1 in the cochlear epithelia is not required in the formation of the scala tympani as suggested by previous reports. In contrast, spiral limbus formation depends on epithelial expression of *Ebf1*, which is surprising. Mesenchyme-specific deletion of *Ebf1* will elucidate how EBF1 forms the spiral limbus. The shorter cochlear duct in $Ebf1^{-/-}$ mice than that in $Foxg1Cre;Ebf1^{fl/fl}$ mice suggests that epithelial EBF1 is not involved in regulating the length of the cochlear duct as well.

More prominent roles of *Ebf1* have been found in the cochlear epithelia. By deleting *Ebf1*, the numbers of both hair and supporting cells increased at E18.5 (Figs. 4, 5). We observed an increase in the numbers of both inner and outer hair cells (Fig. 6). This phenotype suggests that EBF1 is involved in the regulation of hair and supporting cell number during cochlear development. To determine its mechanisms, we evaluated the specifications and differentiation of the cochlear prosensory domain and its proliferation and cell death status under *Ebf1* knock-out conditions. We found that the formation of cochlear nonsensory regions medial and lateral to the prosensory domain were normal in $Ebf1^{-/-}$ mice (Fig. 9*A*), indicating that the phenotypes of $Ebf1^{-/-}$ mouse cochlear sensory epithelia were caused by factors within the prosensory domain. In contrast to markers outside the prosensory domain, the molecules expressed in the prosensory domain and Kölliker's organs, JAG1 and SOX2, showed abnormal expression patterns (Figs. 2, 4*A*, 9*A*). These two molecules were expressed in a more medial region of the $Ebf1^{-/-}$ mouse cochlear duct floor at E14.5 and E18.5. The fact that EBF1 was expressed in a more medial region than SOX2 in wild-type mice indicates that it plays a role in suppressing the localization of JAG1- and SOX2-positive cells in the most medial region. The study of proliferation status within the SOX2-positive cells showed that *Ebf1* deletion enhanced the proliferation of SOX2-positive cells specifically at E13.5 (Fig. 10*D*), which was supported by the loss of CDKN1B expression in the possible prosensory domain of the $Ebf1^{-/-}$ mice at E13.5 (Fig. 10*E*,*F*). The highest *Ebf1* expression level at E13.5 (Fig. 1*A*) may be related to these phenotypes in $Ebf1^{-/-}$ mice. This aberrant proliferation within SOX2-positive cells was suggested to increase the numbers of hair and supporting cells at later stages (Fig. 4*A*,*B*,*D*). Evaluation of hearing ability at the postnatal stage showed that an increase in hair and supporting cell numbers resulted in an increased hearing threshold (Fig. 12). These results indicate that EBF1 suppresses the proliferation of SOX2-positive cells and thus contributes to the development of appropriate numbers of hair and supporting cells, resulting in the development of normal auditory function. Rich expression of EBF1 in SOX2-positive cells within the medial part of the cochlear duct floor, containing the Kölliker's organ (Kolla et al., 2020) and the GER (Kubota et al., 2021), suggests that these regions are involved in the regulation of the hair and supporting cell number. Several lines of evidence support the function of EBF1 to suppress cell proliferation. Human EBF1 has been reported to suppress the proliferation of malignant tumors (Shen et al., 2020), and the deletion of *Rb1*, a known tumor suppressor and cell cycle regulator (Lipinski and Jacks, 1999; Classon and Harlow, 2002), results in the same morphology in the cochlea as that caused by *Ebf1* deletion (Sage et al., 2005). The gain-of-function study will confirm that the regulation of the proliferation is the primary role of EBF1 in the cochlea. Also, gain-of-function approaches in vitro could be used to study the function of EBF1 in its trans-interactions with surrounding mesenchyme cells.

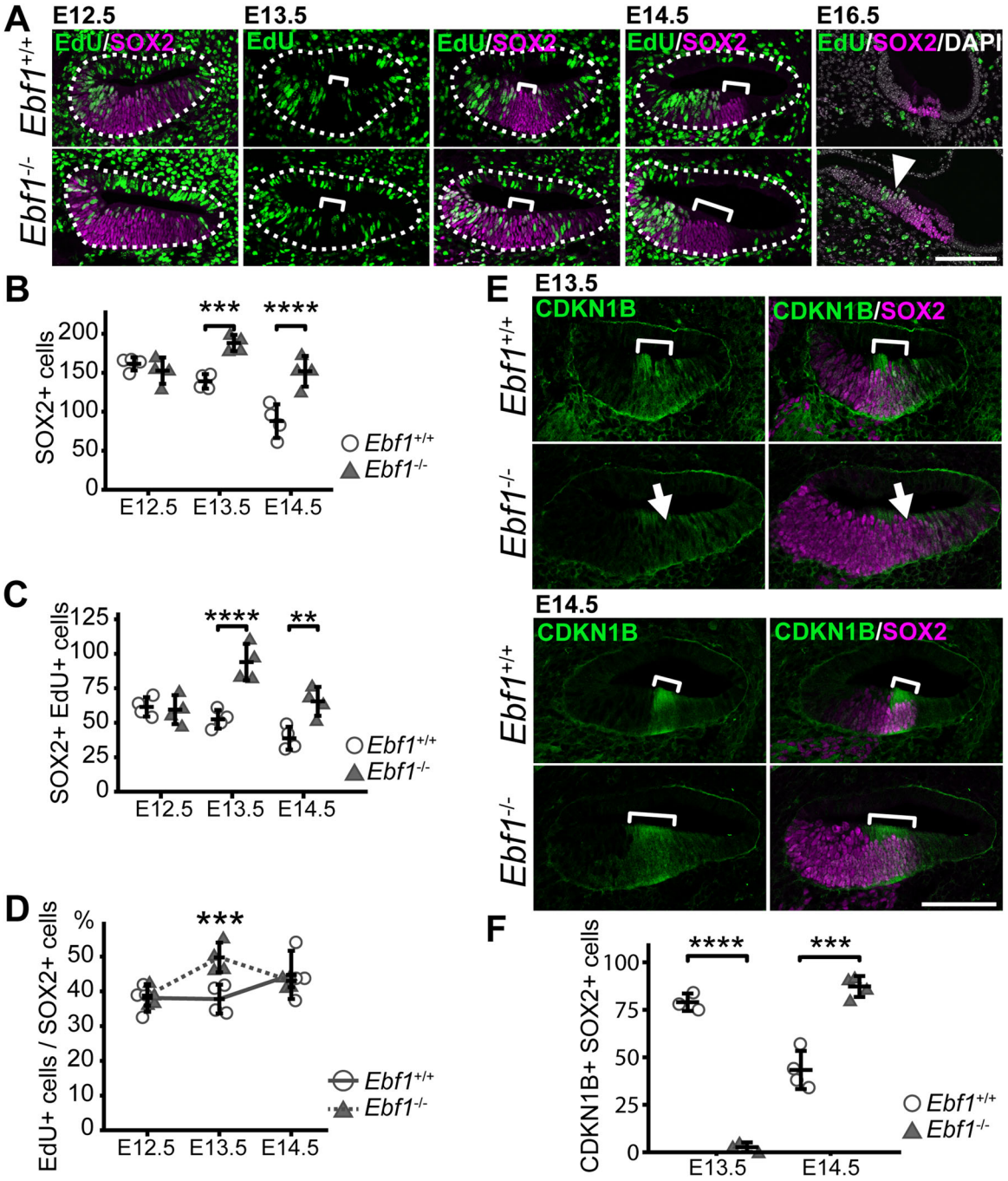

Figure 10. Effect of *Ebf1* deletion on cell proliferation during inner ear development. ***A***, Cross-sections of the cochlear basal regions at E12.5, E13.5, E14.5, and E16.5 from $Ebf1^{+/+}$ and $Ebf1^{-/-}$ mice. Sections were immunostained with 5-ethynyl-2′-deoxyuridine (EdU, green) and SOX2 (magenta). E16.5 sections were counter-stained with 4′,6-diamidino-2-phenylindole (DAPI, gray). Areas enclosed by dashed lines indicate the cochlear ducts and brackets indicate prosensory domains. ***B–D***, Quantitative assessment of the SOX2-positive region in the cochlea epithelia. The numbers of SOX2-positive cells (***B***) as well as EdU- and SOX2-double-positive cells (***C***) were counted, and the percentage of EdU-positive cells among SOX2-positive cells (***D***) was calculated. Error bars represent mean ± standard deviation ($n = 4$). ***E***, Cross-sections of the cochlear basal regions at E13.5 and E14.5 from $Ebf1^{+/+}$ and $Ebf1^{-/-}$ mice immunostained with CDKN1B (green) and SOX2 (magenta). ***F***, Quantitative assessment of the CDKN1B-positive region in the cochlear epithelia. The numbers of CDKN1B- and SOX2-double-positive cells were counted. Two-way ANOVA with Bonferroni's post hoc test (***B–D***) and Student's *t* test (***F***) were performed. $^{**}p < 0.01$, $^{***}p < 0.001$, and $^{****}p < 0.0001$. Error bars represent mean ± standard deviation [$n = 4$ for ***B–D***, ***F*** (E14.5); $n = 3$ for ***F*** (E13.5)]. Scale bar, 100 µm.

The expression of mature cochlear cell markers, including MYO7A, VGULT3, and p75, in $Ebf1^{-/-}$ mice indicated that each cell type developed with normal cell fate specification. Although some GER cells in the *Ebf1*-deleted mouse cochlea ectopically expressed the hair cell marker MYO7A (Fig. 4*B*,*C*), the penetrance of this phenotype was low. Cell fate may be regulated by EBF1 in the cochlea to a small extent; however, cell specification is not a prominent role of cochlear EBF1, which is different from B-lymphocytes (Nechanitzky et al., 2013). In contrast, several results from our study indicate that the differentiation appears to be delayed in the $Ebf1^{-/-}$ mouse cochlea. The expression of *Atoh1* within the cochlear prosensory domain, which was observed at E14.5 in wild-type mice, was detected as late as E15.5 in $Ebf1^{-/-}$ mice (Fig. 9*B*). VGLUT3- and p75-positive cells

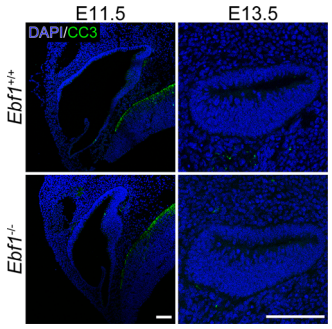

Figure 11. *Ebf1* deletion did not affect apoptosis during inner ear development. Cross-sections of the E11.5 inner ear and E13.5 cochlear basal region from $Ebf1^{+/+}$ and $Ebf1^{-/-}$ mice. Sections were labeled with cleaved caspase 3 (CC3, green) and 4′,6-diamidino-2-phenylindole (DAPI, blue). The number of CC3-positive cells was similar between $Ebf1^{-/-}$ and $Ebf1^{+/+}$ mice at E11.5 and E13.5. Scale bar, 100 µm.

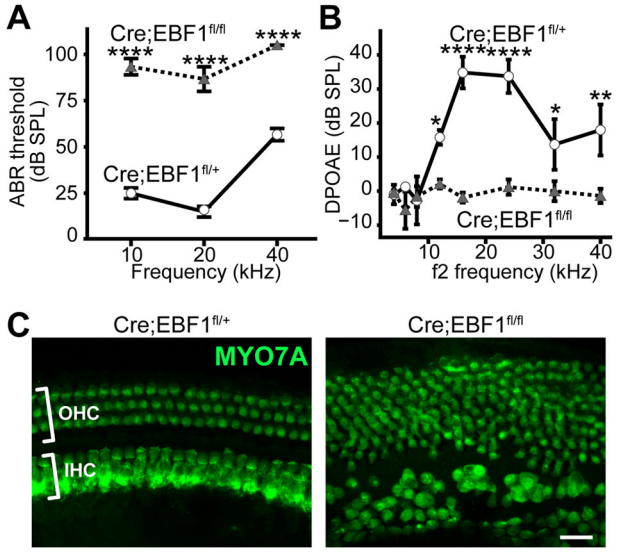

Figure 12. *Ebf1* deletion impairs auditory function. ***A***, ABR thresholds of P21 *Foxg1Cre;* $Ebf1^{fl/fl}$ (Cre;$EBF1^{fl/fl}$; dashed line) and *Foxg1Cre;*$Ebf1^{fl/+}$ (Cre;$EBF1^{fl/+}$, control; solid line) mice. ***B***, DPOAEs were measured at P21 from *Foxg1Cre;*$Ebf1^{fl/fl}$ (dashed line) and control (solid line) mice. $*p < 0.05$, $**p < 0.01$, and $****p < 0.0001$ from one-way ANOVA with Tukey–Kramer post hoc test. Error bars represent mean ± standard error of mean ($n = 3$ for ***A*** and $n = 4$ for ***B***). ***C***, The whole-mount images of the cochlear basal regions from *Foxg1Cre;*$Ebf1^{fl/+}$ and *Foxg1Cre;*$Ebf1^{fl/fl}$ mice at P23 labeled with phalloidin (green). Scale bar, 20 µm.

were not detected in the apical region in $Ebf1^{-/-}$ mouse cochlea at E18.5 (Fig. 6). This delay in differentiation may be caused by the aberrant proliferation of the prosensory domain in $Ebf1^{-/-}$ mice, as the deterioration of proliferation affects the differentiation of cochlear hair cells (Bok et al., 2013; Golden et al., 2015).

An altered neuroaxonal composition of spiral ganglion neuronal cells in the *Ebf1*-deleted organ of Corti (Fig. 8) suggests that EBF1 may affect the pathfinding of spiral ganglion cells within the cochlea, as observed in facial branchiomotor neurons and retina (Garel et al., 2000; Jin and Xiang, 2011). Considering the role of otic mesenchyme in the innervation of spiral ganglion axons on hair cells (Coate and Kelley, 2013), mesenchymal *Ebf1* defect may also contribute to the phenotype observed in the spiral ganglion cells.

The *Ebf1* is expressed in the medial region of the cochlear duct floor (Figs. 1*B*,*C*, 2) and the spiral limbus loss (Fig. 3*C*) and ectopic MYO7A-positive cells within the GER (Fig. 4*B*,*C*) in *Ebf1*-deleted mice are similar to the phenotype of knock-out mice of *Prdm16*, a marker of Kölliker's organ. Moreover, *Prdm16* knock-out mice showed decreased expression of *Ebf1* in the cochlear duct (Ebeid et al., 2022). These support the involvement of EBF1 in the Kölliker's organ development.

The phenotypes of the increased numbers of hair and supporting cells suggest the involvement of molecules crucial for the development of cochlear sensory epithelia, including Notch signal-related molecules (Yamamoto et al., 2011) and SOX2 (Kiernan et al., 2005), in the regulation of *Ebf1* expression. However, that is not the case because *Ebf1* expression levels did not change in striatal neurons of *Foxg1Cre*-mediated *Notch 1*- or *Sox2*-deleted mice (Mason et al., 2005; Ferri et al., 2013). Identification of the molecules upstream and downstream of EBF1 will be the next step in revealing the precise function of EBF1 in the cochlea and the grand scheme of inner ear development.

In conclusion, *Ebf1* and its protein are expressed in the epithelia of the inner ear prosensory domain as well as in Kölliker's organ, the mesenchyme, and CVG cells within the cochlea and play important roles in the formation of each structure. Epithelial EBF1 regulates the number of cochlear hair and supporting cells by suppressing the proliferation of the prosensory domain and Kölliker's organ cells, mainly at E13.5. Therefore, epithelial EBF1 is crucial for normal hearing in mammals.

References

Bermingham-McDonogh O, Oesterle EC, Stone JS, Hume CR, Huynh HM, Hayashi T (2006) Expression of Prox1 during mouse cochlear development. J Comp Neurol 496:172–186.

Bermingham NA, Hassan BA, Price SD, Vollrath MA, Ben-Arie N, Eatock RA, Bellen HJ, Lysakowski A, Zoghbi HY (1999) Math1: an essential gene for the generation of inner ear hair cells. Science 284:1837–1841.

Bok J, Zenczak C, Hwang CH, Wu DK (2013) Auditory ganglion source of Sonic hedgehog regulates timing of cell cycle exit and differentiation of mammalian cochlear hair cells. Proc Natl Acad Sci U S A 110:13869–13874.

Chen P, Johnson JE, Zoghbi HY, Segil N (2002) The role of Math1 in inner ear development: uncoupling the establishment of the sensory primordium from hair cell fate determination. Development 129:2495–2505.

Chen P, Segil N (1999) P27(Kip1) links cell proliferation to morphogenesis in the developing organ of Corti. Development 126:1581–1590.

Classon M, Harlow E (2002) The retinoblastoma tumour suppressor in development and cancer. Nat Rev Cancer 2:910–917.

Coate TM, Kelley MW (2013) Making connections in the inner ear: recent insights into the development of spiral ganglion neurons and their connectivity with sensory hair cells. Sem Cell Dev Biol 24:460–469.

Dayaratne MW, Vlajkovic SM, Lipski J, Thorne PR (2014) Kolliker's organ and the development of spontaneous activity in the auditory system: implications for hearing dysfunction. BioMed Res Int 2014:367939.

Ebeid M, Barnas K, Zhang H, Yaghmour A, Noreikaite G, Bjork BC (2022) PRDM16 expression and function in mammalian cochlear development. Dev Dyn 251:1666–1683.

Ferri A, et al. (2013) Sox2 is required for embryonic development of the ventral telencephalon through the activation of the ventral determinants Nkx2.1 and Shh. Development 140:1250–1261.

Garel S, Garcia-Dominguez M, Charnay P (2000) Control of the migratory pathway of facial branchiomotor neurones. Development 127:5297–5307.

Garel S, Marin F, Grosschedl R, Charnay P (1999) Ebf1 controls early cell differentiation in the embryonic striatum. Development 126:5285–5294.

Golden EJ, Benito-Gonzalez A, Doetzlhofer A (2015) The RNA-binding protein LIN28B regulates developmental timing in the mammalian cochlea. Proc Natl Acad Sci U S A 112:E3864–E3873.

Gyory I, Boller S, Nechanitzky R, Mandel E, Pott S, Liu E, Grosschedl R (2012) Transcription factor Ebf1 regulates differentiation stage-specific signaling, proliferation, and survival of B cells. Genes Dev 26:668–682.

Hagman J, Gutch MJ, Lin H, Grosschedl R (1995) EBF contains a novel zinc coordination motif and multiple dimerization and transcriptional activation domains. EMBO J 14:2907–2916.

Hagman J, Travis A, Grosschedl R (1991) A novel lineage-specific nuclear factor regulates mb-1 gene transcription at the early stages of B cell differentiation. EMBO J 10:3409–3417.

Hamaguchi K, Yamamoto N, Nakagawa T, Furuyashiki T, Narumiya S, Ito J (2012) Role of PGE-type receptor 4 in auditory function and noise-induced hearing loss in mice. Neuropharmacology 62:1841–1847.

Hébert JM, McConnell SK (2000) Targeting of cre to the Foxg1 (BF-1) locus mediates loxP recombination in the telencephalon and other developing head structures. Dev Biol 222:296–306.

Jin K, Xiang M (2011) Ebf1 deficiency causes increase of Müller cells in the retina and abnormal topographic projection at the optic chiasm. Biochem Biophys Res Commun 414:539–544.

Kada S, Nakagawa T, Ito J (2009) A mouse model for degeneration of the spiral ligament. J Assoc Res Otolaryngol 10:161–172.

Kiernan AE, Pelling AL, Leung KKH, Tang ASP, Bell DM, Tease C, Lovell-Badge R, Steel KP, Cheah KSE (2005) Sox2 is required for sensory organ development in the mammalian inner ear. Nature 434:1031–1035.

Kolla L, et al. (2020) Characterization of the development of the mouse cochlear epithelium at the single cell level. Nat Commun 11:2389.

Kubota M, Scheibinger M, Jan TA, Heller S (2021) Greater epithelial ridge cells are the principal organoid-forming progenitors of the mouse cochlea. Cell Rep 34:108646.

Li C, Shu Y, Wang G, Zhang H, Lu Y, Li X, Li G, Song L, Liu Z (2018) Characterizing a novel vGlut3-P2A-iCreER knockin mouse strain in cochlea. Hear Res 364:12–24.

Liberg D, Sigvardsson M, Akerblad P (2002) The EBF/Olf/collier family of transcription factors: regulators of differentiation in cells originating from all three embryonal germ layers. Mol Cell Biol 22:8389–8397.

Lin H, Grosschedl R (1995) Failure of B-cell differentiation in mice lacking the transcription factor EBF. Nature 376:263–267.

Lipinski MM, Jacks T (1999) The retinoblastoma gene family in differentiation and development. Oncogene 18:7873–7882.

Mason HA, Rakowiecki SM, Raftopoulou M, Nery S, Huang Y, Gridley T, Fishell G (2005) Notch signaling coordinates the patterning of striatal compartments. Development 132:4247–4258.

Nechanitzky R, Akbas D, Scherer S, Gyory I, Hoyler T, Ramamoorthy S, Diefenbach A, Grosschedl R (2013) Transcription factor EBF1 is essential for the maintenance of B cell identity and prevention of alternative fates in committed cells. Nat Immunol 14:867–875.

Nieminen-Pihala V, Tarkkonen K, Laine J, Rummukainen P, Saastamoinen L, Nagano K, Baron R, Kiviranta R (2021) Early B-cell Factor1 (Ebf1) promotes early osteoblast differentiation but suppresses osteoblast function. Bone 146:115884.

Ohyama T, Basch ML, Mishina Y, Lyons KM, Segil N, Groves AK (2010) BMP signaling is necessary for patterning the sensory and nonsensory regions of the developing mammalian cochlea. J Neurosci 30: 15044–15051.

Phippard D, Lu L, Lee D, Saunders JC, Crenshaw EB 3rd (1999) Targeted mutagenesis of the POU-domain gene Brn4/Pou3f4 causes developmental defects in the inner ear. J Neurosci 19:5980–5989.

Sage C, et al. (2005) Proliferation of functional hair cells in vivo in the absence of the retinoblastoma protein. Science 307:1114–1118.

Saino-Saito S, Suzuki R, Tokuda N, Abe H, Kondo H, Owada Y (2010) Localization of fatty acid binding proteins (FABPs) in the cochlea of mice. Ann Anat 192:210–214.

Schneider CA, Rasband WS, Eliceiri KW (2012) NIH image to ImageJ: 25 years of image analysis. Nat Methods 9:671–675.

Shen Z, et al. (2020) Transcription factor EBF1 over-expression suppresses tumor growth in vivo and in vitro via modulation of the PNO1/p53 pathway in colorectal cancer. Front Oncol 10:1035.

Sher AE (1971) The embryonic and postnatal development of the inner ear of the mouse. Acta Otolaryngol Suppl 285:1–77.

Taniguchi M, Yamamoto N, Nakagawa T, Ogino E, Ito J (2012) Identification of tympanic border cells as slow-cycling cells in the cochlea. PLoS One 7: e48544.

Urness LD, Wang X, Shibata S, Ohyama T, Mansour SL (2015) Fgf10 is required for specification of non-sensory regions of the cochlear epithelium. Dev Biol 400:59–71.

von Bartheld CS, Patterson SL, Heuer JG, Wheeler EF, Bothwell M, Rubel EW (1991) Expression of nerve growth factor (NGF) receptors in the developing inner ear of chick and rat. Development 113:455–470.

Wang MM, Reed RR (1993) Molecular cloning of the olfactory neuronal transcription factor Olf-1 by genetic selection in yeast. Nature 364: 121–126.

Wu DK, Kelley MW (2012) Molecular mechanisms of inner ear development. Cold Spring Harbor Perspect Biol 4:a008409.

Yamamoto N, Chang W, Kelley MW (2011) Rbpj regulates development of prosensory cells in the mammalian inner ear. Dev Biol 353:367–379.

Yamamoto R, Ohnishi H, Omori K, Yamamoto N (2021) In silico analysis of inner ear development using public whole embryonic body single-cell RNA-sequencing data. Dev Biol 469:160–171.